Ligand requirements for immunoreceptor triggering

Michael I. Barton, Rachel L. Paterson[1], Eleanor M. Denham[2], Jesse Goyette[3,4], P. Anton van der van der Merwe[4,5]

Sir William Dunn School of Pathology, University of Oxford, Oxford OX1 3RE

[1]Current address: Stemmatters, Biotecnologia e Medicina Regenerativa SA, Parque de Ciência e Tecnologia Avepark, Zona Industrial da Gandra, Barco, Portugal

[2]Current address: Enara Bio, The Magdalen Centre, Oxford Science Park, 1 Robert Robinson Avenue, Oxford OX4 4GA

[3]Current address: Department of Molecular Medicine, School of Biomedical Sciences, University of New South Wales, Sydney 2052, NSW, Australia

[4]These authors contributed equally

[5]Correspondence: anton.vandermerwe@path.ox.ac.uk

Abstract

Leukocytes interact physically with other cells using cell surface receptors. The largest group of such receptors are non-catalytic tyrosine phosphorylated receptors (NTRs), also called immunoreceptors. Although NTRs have structurally diverse extracellular domains, they signal by a shared mechanism, involving phosphorylation of cytoplasmic tyrosine residues by SRC-family tyrosine kinases. How ligand binding to NTRs induces this phosphorylation, also called NTR triggering, remains controversial, with roles suggested for size-based segregation, clustering, and mechanical force. Here we exploit a recently developed cell-surface generic ligand system to explore the ligand requirements for NTR triggering. We examine the effect of varying the ligand's length, mobility and valency on the activation of representative members of four NTR families: SIRPβ1, Siglec 14, NKp44 and TREM-1. Increasing the ligand length impairs activation via NTRs, despite enhancing cell-cell conjugation, while varying ligand mobility has little effect on either conjugation or activation. Increasing the valency of the ligand, while enhancing cell-cell conjugation, does not enhance activation at equivalent levels of conjugation. These findings support a role for size-based segregation, rather than mechanical force or clustering, in NTR triggering, consistent with the kinetic-segregation model.

Introduction

The cell surface of an immune cell or leukocyte presents many different receptors, which sense their environment through ligand binding (Barclay et al., 1997; Shilts et al., 2022; Springer, 1990). Many leukocyte receptors bind to ligands on the surface of other cells to mediate adhesion and/or transduce signals which regulate leukocyte function. These signals determine whether the leukocyte ignores or responds to the cell and influence the nature of the response. The largest class of such receptors are non-catalytic tyrosine-phosphorylated receptors (NTRs), which are also called immunoreceptors (Dushek et al., 2012). More than one hundred leukocyte receptors, in more than 20 families, can be classified as NTRs (Dushek et al., 2012). Because they regulate immune cell function, NTRs have roles in a wide range of diseases, and they are being exploited for therapeutic purposes. For example, synthetic NTRs (e.g. chimeric antigen receptors) and antibodies targeting NTRs or their ligands (e.g. checkpoint inhibitors) have become standard therapies for several forms of cancer (June and Sadelain, 2018; Sharma and Allison, 2015).

While NTRs have structurally diverse extracellular regions they all have, or are associated with signalling subunits that have, conserved tyrosine containing motifs in their cytoplasmic domains, such as the immunoreceptor tyrosine-based activation motif (ITAM) and immunoreceptor tyrosine-based switch motif (ITSM) (Dushek et al., 2012). These motifs are phosphorylated by SRC-family tyrosine kinases,

which are tethered via acyl groups to the inner leaflet of the plasma membrane. This phosphorylation is regulated by the receptor tyrosine phosphatases CD45 and CD148, which act on both SRC-kinases and their substrates. While the extracellular regions of NTRs are structurally diverse, they are typically smaller (4-10 nm) than many abundant cell surface molecules such as CD43, CD44, CD45, CD148 and integrins, which range in size from 21-50 nm. When these size differences were first noted for the TCR and its peptide-MHC (pMHC) ligand it was predicted that, when T cells contacted other cells, there would be segregation of the TCR/pMHC complex from larger molecules like CD45 (Springer, 1990). This observation, together with evidence that constitutive tyrosine phosphatase activity suppresses TCR triggering in resting cells (O'Shea et al., 1992; Secrist et al., 1993), led to the proposal that TCR binding to pMHC induced tyrosine phosphorylation of the TCR by trapping it in small regions of close contact which exclude large receptor tyrosine phosphatases CD45 and CD148 but not the SRC-kinases (Davis and van der Merwe, 1996). This mechanism was subsequently termed the kinetic segregation (KS) model (van der Merwe et al., 2000). Subsequent studies from multiple laboratories using a wide range of techniques have demonstrated that the KS mechanism plays a key role in TCR triggering (Burroughs et al., 2006; Chang et al., 2016; Chen et al., 2021; Choudhuri et al., 2005; Cordoba et al., 2013; James and Vale, 2012; Jenkins et al., 2023; Razvag et al., 2018; Schmid et al., 2016; Varma et al., 2006; Wilhelm et al., 2021). Recently it has been shown that synthetic receptors based on the TCR, namely chimeric antigen receptors (CARs), also appear to trigger by the KS mechanism, which has important implications for the design of these receptors and selection of their target antigens (Xiao et al., 2022). Other mechanisms that been proposed to contribute to TCR triggering are aggregation (Goyette et al., 2019) or conformational change, with conformational change being either allosteric (Schamel et al., 2019) or induced by mechanical force (Ma et al., 2008; Zhu et al., 2019).

The similarities in signalling between the TCR and other NTRs have led to the hypothesis that the KS mechanism may contribute to triggering by other NTRs (Davis and van der Merwe, 2006; Dushek et al., 2012). Indeed, evidence for this has been reported for NKG2D in NK cells (Köhler et al., 2010), Dectin-1 (Goodridge et al., 2011) and FcyRs (Bakalar et al., 2018) in macrophages, and CD28 in T cells (Lim et al., 2015). However, the diversity of NTRs and their ligands, and the fact that many NTR ligands have yet to be identified, has hampered investigation of the triggering mechanism in a wider range of NTRs. We have recently developed a generic ligand system based on the SpyTag/SpyCatcher split protein, which enables cell-surface Streptactin to be used to engage any NTR incorporating a membrane-distal StrepTagII peptide (Denham et al., 2019). Importantly, this generic ligand stimulated TCRs at the same surface density as the native TCR ligand, validating it as a suitable model system for investigating NTR triggering (Denham et al., 2019).

In the present study we used this generic ligand system to explore the ligand requirement for triggering by representative members of 4 distinct NTR families (Figure 1A): Signal regulatory protein β1 (SIRPβ1), Sialic acid-binding immunoglobulin-type lectin 14 (Siglec 14), Natural killer receptor 44 (NKp44) and Triggering receptor expressed on myeloid cells 1 (TREM-1). SIRPβ1 is highly homologous to the inhibitory receptor and therapeutic target SIRPα (Kharitonenkov *et al.*, 1997). SIRPβ1 and SIRPα are examples of paired activatory/inhibitory NTRs (Dushek et al., 2012), with conserved extracellular regions but distinct transmembrane and cytoplasmic domains. The native ligand of SIRPβ1 is unknown but it is thought to promote phagocytosis in macrophages (Hayashi *et al.*, 2004). Siglec 14 is a member of the sialic acid-binding Siglec family of receptors (Angata et al., 2006; Crocker et al., 2007). Siglec 14 and Siglec 5 are paired activatory and inhibitory NTRs, respectively (Angata *et al.*, 2006). NKp44 is important for the activation and cytotoxic activity of natural killer cells and reportedly binds a wide range of ligands (Parodi et al., 2019). Finally, TREM-1 is an activatory member of a family of NTRs (Ford and McVicar, 2009) that has been reported to bind peptidoglycan recognition protein 1 (PGLYRP1) (Read *et al.*, 2015) and extracellular actin (Fu *et al.*, 2017). All four receptors associate with, and presumably signal using, the ITAM-containing adaptor protein DAP12 (Lanier and Bakker, 2000).

To investigate the triggering mechanism used by these NTRs we examined the effect of changing ligand size, mobility, and valency on activation. Elongating the ligand inhibited activation via these receptors despite enhancing receptor/ligand mediated cell-cell conjugation. In contrast, changing the ligand mobility had little effect on conjugation or activation. Finally, while increasing the ligand valency increased cell-cell conjugation as well as activation, multivalent ligand lower levels of activation at equivalent levels of cell-cell conjugation. Taken together, these result support a role for the KS mechanism in triggering by these NTRs, and argue against roles for mechanical force or clustering.

Results

Varying ligand length

In the SpyTag-SpyCatcher system a covalent (isopeptide) bond spontaneously forms between Spytag and SpyCatcher when they are mixed together (Zakeri *et al.*, 2012). In our previously described generic ligand system (Denham et al., 2019), SpyTag is fused to the N-terminus of a transmembrane protein expressed on ligand-presenting CHO cells, forming the ligand anchor, while SpyCatcher is fused to a Strep-Tactin tetramer, which can have between one and four active binding sites, as required (Figure 1A). The receptor is modified at its membrane-distal N-terminus to contain a Strep-tag II peptide, which binds monovalent Strep-Tactin with a K_D of 43 μM (Denham et al., 2019). This is within the affinity range typical of leukocyte cell-cell interactions (van der Merwe and Barclay, 1994; Shilts et al., 2022).

To test the effect of ligand length on activation via NTRs, we produced CHO cells expressing either a short or a long ligand anchor, where the latter includes a ~11 nm spacer comprising the four Ig domains of CD4 (Figure 1A) (Wu et al., 1997). By titrating the monovalent Strep-Tactin SpyCatcher we produced a panel of CHO cells with a range of binding sites. We used a previously described method to accurately quantify the number of Strep-Tactin binding sites presented by these cells (Denham et al., 2019). This involved measuring the maximum number of biotin binding sites and the K_D for Strep-Tactin SpyCatcher coupling to cells (sFigure 1) and using these parameters to calculate the number of binding sites, as described in the Materials and Methods.

We first measured the impact of ligand elongation on the receptor engagement using a cell-cell conjugation assay as a readout. For receptor cells we used monocytoid THP-1 cells expressing the SIRPβ1 receptor with an N-terminal Strep-tag II peptide. The conjugation assay involves mixing receptor and ligand cells stained with different fluorescent dyes and measuring double positive events by flow cytometry (Figure 1B, upper right quadrants). As expected, reducing the number of binding sites resulted in a decrease in the percentage of receptor cells in conjugates (Figure 1B).

We then compared the conjugation efficacy of SIRPβ1 THP-1 cells mixed with short or long CHO cells presenting different numbers of binding sites. When plotting conjugates against binding sites, cells presenting the long ligand produced more conjugates (Figure 1C, left panel). This suggests that increasing the ligand length promotes conjugate formation, which is consistent with other studies suggesting that increasing the length of short (< 8 nm) cell surface ligands improves receptor engagement (Choudhuri et al., 2005; Lim et al., 2015; Wild et al., 1999).

We next examined the effect of ligand length on SIRPβ1 mediated IL-8 production. Interestingly the long ligand stimulated less IL-8 production than the short ligand (Figure. 1C, middle panel), despite mediating improved conjugate formation. To normalise for differences in conjugate formation we plotted the functional IL-8 response against the percentage of receptor cells in conjugates (Figure 1C, right panel). This confirmed that, at equivalent levels of conjugate formation, the long ligand induced lower levels of IL-8 production.

We performed conjugation and stimulation assays on other NTRs (Siglec 14, NKp44 and TREM-1) using the short or long generic ligand (Figure 2). As in the case of SIRPβ1, the results for NKp44 and TREM-1 show an increase in conjugation efficacy when binding to the long ligand compared to the short ligand (Figure 2, left panels). This was not the case for Siglec 14, where no difference was seen (Figure 2B, left panel). Elongation of the ligand impaired activation of IL-8 release via all four NTRs, both before and after normalising for conjugate formation (Figure 2, centre and right panels, respectively).

One likely explanation for the effect of ligand length on activation efficiency is that increasing the ligand length increases the length of the NTR/ligand complex. If this is the case, activation should also be reduced by increasing the length of the NTRs. The extracellular regions of SIRPβ1 and Siglec 14 each contain 3 immunoglobulin superfamily (IgSF) domains, whereas the extracellular regions of NKp44 and TREM-1 only have 1 IgSF domain (Figure 1A). To examine whether this size difference had a measurable impact we reanalysed the data in Figure 2 to enable comparison of conjugation and activation via NTRs exposed to the same ligand (sFigure 3). Short NTRs (NKp44 and TREM-1) mediated lower levels of conjugation (sFigure 3, left panels) but high levels of stimulation when normalised for conjugation (sFigure 3, right panels), and this was observed with both short (sFigure 3A) and long (sFigure 3B) ligands. Taken together, these data show that elongation of these NTR/ligand complexes abrogates activation via these four NTRs.

Varying ligand mobility

We next examined the effect of varying the ligand anchor on NTR activation. We compared ligand anchors based on the transmembrane and cytoplasmic domains of CD80, and CD43 and the glycosylphosphatidylinositol (GPI) anchor of CD52. The CD43 cytoplasmic domain interacts with the actin cytoskeleton though Ezrin/Radixin/Moesin (ERM) proteins (Yonemura *et al.*, 1998), and so is likely to be more firmly anchored. In contrast, CD52 is a GPI anchored protein and thus less firmly anchored, and presumably more mobile (Figure 3A). To examine mobility, SpyCatcher-GFP was coupled to ligand anchors and fluorescence recovery after photobleaching (FRAP) performed. As expected, the CD52 anchor conferred greater mobility than the CD80 or CD43 anchor, which were similar (Figure 3B).

We next compared the effect of changing the ligand mobility on conjugation with and stimulation of SIRPβ1 expressing THP-1 cells. It was not possible to attain as high a level of binding sites on the CD43 and CD52 ligand anchor cells but comparison was possible over a reasonable range. Both CD52 and CD43 anchored ligands induced similar levels of conjugate formation and IL-8 release at comparable levels of binding sites (Figures 3C and D). There was a difference between the CD52 and CD43 anchors when IL-8 release was plotted against levels of conjugation (Figure 3E). However this difference was small and could be the result of faster turnover of the CD52 anchored ligand (sFigure 5), which would reduce engagement during the 20 h stimulation. While the CD80 anchored ligand was less potent at mediating conjugation and IL-8 release, this was not a consequence of differences in lateral mobility. Taken together, these results suggest that changes in the ligand mobility do not affect SIRPβ1 mediated conjugation or triggering.

Varying ligand valency

Since ligand-induced clustering of receptors is often assumed to be the mechanism of receptor-activation, we next examined the effect of increasing the valency of the ligand from 1 to 4 by using a tetravalent form of Strep-Tactin Spycatcher (Figure 1A). As expected, conjugation with tetravalent instead of monovalent Strep-Tactin Spycatcher resulted in a four-fold increase in the number of binding sites (sFigure 6). We then compared the ability of monovalent and tetravalent ligand to mediate conjugation and induce IL-8 secretion from THP-1 cells expressing the 4 different NTRs. Tetravalent ligand induced conjugation via all 4 NTRs at lower ligand binding site numbers than monovalent ligand (Figure 4, left panels), indicating that increasing the ligand valency increases NTR binding, presumably by increasing avidity. Increasing the valency enabled activation of all four receptors, as measured by IL-8 release, at much lower ligand binding sites (Figure 4, middle panels). However, when we controlled for increased conjugate formation, tetravalent ligand was less effective than monovalent ligand at stimulating IL-8 release at equivalent levels of conjugation (Figure 4, right panels). The same result was observed with the CD80, CD43 and CD52 ligand anchors (sFigure 7 and 8). These results indicate that, while increasing the valency of a cell surface-associated ligand enhances binding to NTRs, it does not increase activation via NTRs.

We next investigated whether activation of NTR by the high avidity tetravalent Strep-Tactin SpyCatcher was sensitive to ligand length. THP-1 cells expressing four representative NTRs were exposed to CHO cells presenting tetravalent Strep-Tactin SpyCatcher on either short or long CD80 anchors (Figure 5). The short ligands were less effective at mediating conjugation than the long ligand for two (SIRPβ1 & NKp44) of the four NTRs (Figure 5, left panels), but more effective at stimulating IL-8 production for three of the four NTRs (SIRPβ1, NKp44 and TREM-1), both before (Figure 5, centre panels) and after (Figure 5, right panels) controlling for conjugate formation. These results show that even high avidity NTR/ligand interactions remain sensitive to ligand length.

Discussion

We have exploited our previously described generic cell surface ligand system (Denham et al., 2019) to explore the effects of varying ligand length, mobility, and valency on activation of four representative NTRs, SIRPβ1, Siglec-14, NKp44 and TREM-1. One advantage of this system is that it enables titration of ligand surface density, enabling detection of quantitative differences in the ability of cell-surface ligands to mediate conjugation and stimulation. A second advantage is that it enables multiple NTRs to be assessed using the same set of ligands, increasing throughput and facilitating comparisons between NTRs. A third advantage is that it enables analysis of orphan NTRs, such as SIRPβ1, whose ligand has yet to be identified.

Our first key finding is that elongation of generic ligands abrogated activation of all four NTRs. This was not a consequence of decreased binding as elongated ligands mediate enhanced cell-cell conjugation. While this contrasted with results in a supported lipid bilayer (SLB) system, in which elongation of CD48 abrogated CD2 binding (Milstein et al., 2008), it is consistent with results obtained with cell surface expressed ligands, including CD48 (Choudhuri et al., 2005; Köhler et al., 2010; Lim et al., 2015; Wild et al., 1999). A likely explanation for this is that ligands on cell surfaces, unlike ligands on SLBs, are crowded by the larger molecules present at high densities. Our finding that long NTRs were less effectively activated than short NTRs suggest that the increased NTR/ligand length abrogates NTR signalling. These data are most consistent with the KS mechanism of NTR triggering (Davis and van der Merwe, 2006), since increasing the NTR/ligand length would be expected to increase the intermembrane distance and thus reduce segregation of inhibitory receptor tyrosine phosphatases such as CD45 from the engaged NTR (Choudhuri et al., 2005). Numerous studies have confirmed that increasing receptor/ligand length abrogates CD45 segregation from engaged NTRs (Al-Aghbar et al., 2018; Bakalar et al., 2018; Chen et al., 2017; Choudhuri et al., 2005; Lim et al., 2015; Xiao et al., 2022). In one of these studies an elongated high affinity TCR ligand, derived from the OKT3 monoclonal antibody, was able to activate TCRs despite less efficient exclusion of CD45 (Al-Aghbar et al., 2018). However, no titration of the ligand number was performed, and a lower affinity variant of the same ligand was unable to activate T cells (Al-Aghbar et al., 2018).

An alternative explanation for our finding that elongation abrogates activation through NTRs is that this could decrease the level of force experienced by the NTR upon ligand engagement (Li et al., 2010). These data are therefore also consistent with models of NTR triggering postulating that a mechanical force imposed upon ligand binding alters the conformation of the NTR (Ma et al., 2008; Zhu et al., 2019). However, whether changing ligand length affects the force experienced by an NTR has yet to be confirmed, and it remains unclear how such a conformational change of NTRs could be transmitted through the membrane to enhance phosphorylation of their cytoplasmic domains. Such a mechanism is difficult to reconcile with enormous structural variability of NTRs (Dushek et al., 2012) and the fact that chimeric NTRs such as CARs tolerate extensive variation in the regions (hinge, transmembrane and cytoplasmic domains) that couple their ligand binding domains with their tyrosine-containing signalling motifs (Labanieh and Mackall, 2023; Sadelain, 2016).

A second key finding is that changing the mobility of the ligand anchor had little impact on its ability mediate activation via NTRs. The CD52 anchor comprises a lipid (GPI) which we show confers greater lateral mobility. A lipid anchor also allows a ligand to be more easily extracted from the plasma membrane by force. Thus, the amount of force that can be exerted on an NTR, both tangential and perpendicular to the membrane, should be lower with lipid-anchored than a transmembrane-anchored

ligand. Furthermore, CD43 is potentially able to bind to the actin cytoskeleton through ERM proteins, which would further increase the force that can be exerted before the ligand is extracted from the cell surface. Thus, our finding that CD43 and CD52 anchors were similarly effective at activating an NTR argues against a substantial role for mechanical force in NTR triggering. In support of this, changing the lateral mobility of the TCR ligand in an SLB system had no effect on TCR triggering despite substantially changing the force experienced by the TCR (Göhring et al., 2021).

The third key finding is that increasing the valency of the NTR ligand did not increase activation of the NTR at equivalent levels of cell-cell conjugation. This result contrasts with the findings obtained with soluble NTR ligands such as cross-linked antibodies and natural ligands engineered to be multivalent, where increasing the valency is required for NTR triggering (Boniface et al., 1998; Cochran et al., 2000). One possible explanation for this discrepancy between the effect of valency with soluble and surface associated ligand is that a soluble multivalent ligand could, by forming clusters of NTRs, exclude molecules with bulky ectodomain, such as CD45, from clustered NTRs, whereas soluble monovalent ligands are unable to do this. In contrast, even a monovalent surface-associated ligand can trap the NTR in zones of a close intermembrane contact from which CD45 and CD148 are excluded. While our finding that tetravalent ligands are less effective at activating NTRs than monovalent ligands requires confirmation and further analysis, the fact that increased valency does not enhance NTR triggering is strong evidence against aggregation as a mechanism of physiological NTR triggering. Further evidence against this model is that almost all cell surface NTRs ligands that have been identified to date are monovalent (Dushek et al., 2012). In contrast, cell surface receptors known to signal by binding induced multimerisation, such as class III tyrosine kinase receptors (Ullrich and Schlessinger, 1990) and TNF receptor superfamily members (Locksley et al., 2001), typically have multivalent ligands.

Our finding that elongation of a tetravalent generic ligand did not impair activation via Siglec 14, while it did impair activation via the three other NTRs, suggests that, for some NTRs, increasing ligand valency can bypass the need for the KS mechanism. It is noteworthy that some Siglec family members, including the Siglec-14 paired receptor Siglec-5 (Cornish et al., 1998), are able to form disulphide linked dimers. Dimeric Siglec-14 would allow formation of large 'zipper-like' aggregates with tetravalent generic ligand, enabling exclusion of CD45 and CD148 without needing the KS mechanism.

Taken together, our finding that activation via NTRs is abrogated by ligand elongation and aggregation and unaffected by the mobility of the ligand anchor supports our hypothesis that NTRs signal by the KS mechanism. While our results focus only on four representative NTRs, these results are likely to apply to a larger number of NTRs, including other members of the Siglec and TREM families and NTRs from other families that signal via the DAP-12 adaptor (Lanier, 2008). As reviewed in the Introduction, there is

already evidence that many NTRs that do not associate with DAP12, including the TCR, NKG2D, CD28, and FcγR, exploit the KS mechanism for triggering. Taken together with the results presented in this paper, this demonstrates that the KS mechanism is used by NTRs which signal through intrinsic tyrosine motifs (CD28, FcγRI and FcγRII) and a variety of signalling subunits (DAP12, DAP10, CD3δεγ, CD247, and FcRγ).

One limitation of the present work is that we used artificial ligands rather than native ligands. Our recent development of Combicells (Patel et al., 2023), which exploit the SpyCatcher/SpyTag system to present native ligand on antigen presenting cells should enable our key results to be confirmed with native ligands, where known. A second limitation, which is a consequence of the system used, is lack of imaging data of the interface between THP-1 cells and CHO cells. Advanced microscopy, beyond the scope of this study, is likely needed to image the molecular events in the microvilli-like structures and close contact areas involved in NTR triggering at cell-cell interfaces (Jenkins et al., 2023; Jung et al., 2021; Stinchcombe et al., 2023).

Material and Methods

Constructs

Receptors

Receptor sequences for SIRPβ1, Siglec 14, NKp44 and TREM-1 were inserted into the pHR-SIN-BX-Strep-tag II plasmid as described by (Denham *et al.*, 2019). The same constructs containing the DAP12 adaptor protein was also used.

Ligand anchors

For the ligand anchors DNA encoding the Igk leader sequence (bold), HA tag (italics), SpyTag (underlined) bracketed by GGS linkers, and the hinge, transmembrane and intracellular regions of mouse CD80, mouse CD43, or human CD52 (italics underlined) was inserted into the vector pEE14. To express the long ligand anchor DNA encoding human CD4 (italics bold) was inserted between the SpyTag and CD80 hinge. This included an R to D point mutation (underlined) to prevent CD4 binding MHC class II. After expression CD52 anchor is cleaved and linked to GPI anchor at the serine residue marked in bold

CD80 anchor (short):

M E T D T L L L W V L L L W V P G S T G D *Y P Y D V P D Y A* T G G S A H I V M V D A Y K P T K G G S G G S *H V S E D F T W E K P P E D P P D S K N T L V L F G A G F G A V I T V V V I V V I I K C F C K H R S C F R R N E A S R E T N N S L T F G P E E A L A E Q T V F L*

CD80 anchor (long):

M E T D T L L L W V L L L W V P G S T G D *Y P Y D V P D Y A* T G G S A H I V M V D A Y K P T K G G S G G S ***K V V L G K K G D T V E L T C T A S Q K K S I Q F H W K N S N Q I K I L G N Q G S F L T K G P S K L N D*** **D** ***A D S R R S L W D Q G N F P L I I K N L K I E D S D T Y I C E V E D Q K E E V Q L L V F G L T A N S D T H L L Q G Q S L T L T L E S P P G S S P S V Q C R S P R G K N I Q G G K T L S V S Q L E L Q D S G T W T C T V L Q N Q K K V E F K I D I V V L A F Q K A S S I V Y K K E G E Q V E F S F P L A F T V E K L T G S G E L W W Q A E R A S S S K S W I T F D L K N K E V S V K R V T Q D P K L Q M G K K L P L H L T L P Q A L P Q Y A G S G N L T L A L E A K T G K L H Q E V N L V V M R A T Q L Q K N L T C E V W G P T S P K L M L S L K L E N K E A K V S K R E K A V W V L N P E A G M W Q C L L S D S G Q V L L E S N I K V L P T R S*** *H V S E D F T W E K P P E D P P D S K N T L V L F G A G F G A V I T V V V I V V I I K C F C K H R S C F R R N E A S R E T N N S L T F G P E E A L A E Q T V F L*

CD43 anchor:

M E T D T L L L W V L L L W V P G S T G D *Y P Y D V P D Y A T G G S* A H I V M V D A Y K P T K G G S G G S *Q E S S G M L L V P M L I A L V V V L A L V A L L L L W R Q R Q K R R T G A L T L S G G G K R N G V V D A W A G P A R V P D E E A T T T S G A G G N K G S E V L E T E G S G Q R P T L T T F F S R R K S R Q G S L V L E E L K P G S G P N L K G E E E P L V G S E D E A V E T P T S D G P Q A K D E A A P Q S L*

CD52 anchor:

M E T D T L L L W V L L L W V P G S T G D *Y P Y D V P D Y A T* G G S A H I V M V D A Y K P T K G G S G G S *S D T S Q T S S P* ***S*** *A S S N I S G G I F L F F V A N A I I H L F C F S*

Soluble proteins

Strep-Tactin-SpyCatcher sequence:

Strep-Tactin is underlined, SpyCatcher is in italics and the polyaspartate sequence is in bold.

M A E A G I T G T W Y N Q L G S T F I V T A G A D G A L T G T Y V T A R G N A E S R Y V L T G R Y D S A P A T D G S G T A L G W T V A W K N N Y R N A H S A T T W S G Q Y V G G A E A R I N T Q W L L T S G T T E A N A W K S T L V G H D T F T K V K P S A A S **D D D G D D D G D D D D** *S A T H I K F S K R D E D G K E L A G A T M E L R D S S G K T I S T W I S D G Q V K D F Y L Y P G K Y T F V E T A A P D G Y E V A T A I T F T V N E Q G Q V T V N G K A T K G D A H I*

Strep-Tactin sequence:

M A E A G I T G T W Y N Q L G S T F I V T A G A D G A L T G T Y V T A R G N A E S R Y V L T G R Y D S A P A T D G S G T A L G W T V A W K N N Y R N A H S A T T W S G Q Y V G G A E A R I N T Q W L L T S G T T E A N A W K S T L V G H D T F T K V K P S A A S

Dead Streptavidin sequence:

Bold amino acids mark substitutions in order to prevent binding to Strep tag II or biotin.

M A E A G I T G T W Y **A** Q L G **D** T F I V T A G A D G A L T G T Y E **A** A V G A E S R Y V L T G R Y D S A P A T D G S G T A L G W T V A W K N N Y R N A H S A T T W S G Q Y V G G A E A R I N T Q W L L T S G T T E A N A W K S T L V G H D T F T K V K P S A A S

GFP-SpyCatcher

The GFP-SpyCatcher construct was described in (Denham *et al.*, 2019).

THP-1 cell lines

THP-1 cells were maintained in RPMI-1640 media (Sigma-Aldrich #R8758) supplemented with 10% foetal bovine serum (FBS) and 1 in 100 penicillin/streptomycin (Thermo Fisher Scientific #15140122) at 37 °C in a 5% CO2 containing incubator.

CHO cell lines

Chinese Hamster Ovary (CHO) mock cells were maintained in DMEM (Sigma-Aldrich #D6429) supplemented with 5% FBS and 1 in 100 penicillin/streptomycin. CHO ligand anchor cells (short and long) were maintained in L-Glutamine-free DMEM (Sigma-Aldrich #D6546) supplemented with 10% dialysed FBS (dialysed three times against 10 L PBS), 1 in 100 penicillin/streptomycin, 1x GSEM supplement (Sigma-Aldrich #G9785) and 50 µM L-Methionine sulfoximine (Sigma-Aldrich #M5379).

Lentiviral transduction of THP-1 cells

Either receptor-expressing lentivector alone, or with the DAP12 adaptor-expressing lentivector, was co-transfected with the lentiviral packaging plasmids pRSV-Rev (Addgene plasmd #12253), pMDLg/pRRE (Addgene plasmd #12251) and pMD2.g (Addgene plasmd #12259) into HEK293T cells using X-tremeGENETM HP (Sigma-Aldrich 6366546001) as per the manufacturer's instructions. Two days after transfection, viral supernatants were harvested, filtered (0.45 µM syringe filter) and used for the transduction of THP-1 cells in the presence of 5 µg mL^{-1} Polybrene.

Analysing receptor and adaptor expression using flow cytometry and cell sorting by Fluorescence-Activated Cell Sorting (FACS)

Cells were analysed for receptor surface expression by flow cytometry using anti-Strep-tag II antibody Oyster 645 (IBA Lifesciences #2-1555-050), or anti-Strep-tag II antibody (IBA Lifesciences #2-1507-001) and anti-mouse IgG1 antibody Alexa Fluor 647 (Thermo Fisher Scientific #A-21240), on a Cytek DxP8. Introduced adaptor expression was tested via expression of EmGFP encoded on the adaptor lentivector. Cells were sorted for matched high expression of receptor plus introduced adaptor by fluorescence-activated cell sorting (FACS) (MoFlo Astrios, Beckman Coulter).

Transfection of CHO cells with various ligand anchors

CHO cells were transfected with either pEE14 (CHO mock) or pEE14-ligand anchor (CHO ligand anchor) using Xtreme-GENE 9™ as per the manufacturer's instructions. Transfected lines were cultured in the appropriate selection media after 48 hours.

Checking ligand anchor expression by flow cytometry

CHO Cells were analysed for ligand anchor surface expression by flow cytometry using anti-HA-Tag antibody Alexa Fluor 647 (6E2; Cell Signalling Technology). Alternatively, cells were coupled with saturating concentration of monovalent StrepTactin SpyCatcher. Biotin ATTO 647 was then added at 2 µM for 30 minutes. The cells were washed 3 times in PBS 1%BSA before they were fixed in PBS 1% formaldehyde and analysed via flow cytometry.

Expression and purification of monovalent and tetravalent Strep-Tactin-SpyCatcher

Strep-Tactin SpyCatcher and dead streptavidin (monovalent) or Strep-Tactin SpyCatcher and Strep-Tactin (tetravalent) expressed in Escherichia coli BL21-CodonPlus (DE3)-RIPL cells (Agilent Technologies #230280) were combined and refolded from inclusion bodies. Inclusion bodies were washed in BugBuster (Merck Millipore #70921) supplemented with lysozyme, protease inhibitors, DNase I and magnesium sulphate as per the manufacturers' instructions. Subunits were then mixed at a 3:1 molar ratio to improve the yield of the desired tetramer. The subunits were refolded by rapid dilution in cold PBS and contaminates removed via precipitation using ammonium sulphate before additional ammonium sulphate was added to precipitate the desired tetramer. Precipitated protein was resuspended in 20 mM Tris pH 8.0, filtered (0.22 µm syringe filter), and loaded onto a Mono Q HR 5/5 column (GE Healthcare Life Sciences). Desired tetramers were eluted using a linear gradient of 0-0.5 M NaCl in 20 mM Tris pH 8.0, concentrated, and buffer exchanged into 20 mM MES, 140 mM NaCl pH 6.0 (Denham *et al.*, 2019).

Coupling CHO generic ligand cells

Ligand anchor expressing or mock transduced CHO cells were incubated with various concentrations of monovalent or tetravalent Strep-Tactin SpyCatcher in 20 mM MES, 140 mM NaCl, pH 6.0 and 1% BSA for 10 minutes at RT. Unbound Strep-Tactin SpyCatcher was removed by washing three times with PBS 1% BSA.

FACS Sorting of ligand anchor expressing CHO cells

CHO short and long cells were coupled with a saturating concentration of monovalent Strep-Tactin SpyCatcher. Biotin ATTO 647 (ATTO-TEC #AD 647-71) was then added at 2 µM for one hour and the excess washed off with PBS 1 % BSA. The short and long CHO cells were then sorted for matched expression of atto 647 signal corresponding to the expression level of ligand anchor using FACS (MoFlo Astrios, Beckman Coulter).

Biotin-4-fluorescein quenching assay

The valency of purified monovalent and tetravalent Strep-Tactin SpyCatcher was measured using biotin-4-fluorescein (Sigma-Aldrich #B9431-5MG) which when bound to Strep-Tactin become quenched. Monovalent and tetravalent Strep-Tactin SpyCatcher was incubated with a titration of biotin-4-fluorescein in black, opaque plates for 30 minutes at RT in PBS 1% BSA. Fluorescence was measured (λ_{ex} 485 nm, λ_{ex} 520 nm) using a plate reader. Fluorescence values were corrected for background fluorescence before analysis. Negative control (buffer alone) data were fitted with the linear regression. Sample data was fitted with a segmental linear regression, equation below, where X is the biotin-4-fluorescein concentration, Y is fluorescence (AU), X0 is the biotin-4-fluorescein concentration at which the line segments intersect. Slope1 was constrained to zero and is the gradient of the first line segment, slope2 is the gradient of the second line segment. Intercept1 was constrained to zero and is the Y value at which the first line segment intersects the Y axis. Slope2 was constrained to the gradient given by the linear regression of the negative control.

$$Y1 = Intercept\ 1 + Slope1 * X$$

$$Y\ at\ X0 = Slope1 * X0 + Intercept1$$

$$Y2 = Y\ at\ X0 + Slope2 * (X - X0)$$

$$Y = IF\ (X < X0, Y1, Y2)$$

The X0 value was converted into an estimate of the number of biotin-binding sites per tetramer using the concentration of Strep-Tactin SpyCatcher added and assuming complete binding of biotin-4-fluorescein.

Measurement of ligand binding sites on cells

Ligand-anchor expressing or mock transduced CHO cells (3 x 10^6) were pre-incubated with a saturating concentration of monovalent or tetravalent Strep-Tactin SpyCatcher. The above biotin-4-fluorescein quenching assay was performed in the same manner but with a known number of cells. The X0 term (calculated from the curve fit using equations above) was converted to the average number of binding sites per cell using the equation below, where N is the average number of ligands per cell, X0 is the saturation concentration of biotin-4-fluorescein extracted (M), V is the sample volume (L), N_A is Avogadro's constant and C is the number of cells in the sample.

$$N = \frac{X0 * V * N_A}{C}$$

To measure relative levels of coupled SpyCatcher per cell, ligand cells were pre-incubated with a range of concentrations of monovalent or tetravalent Strep-Tactin SpyCatcher or buffer alone (as a negative control) before being incubated with 2 µM biotin ATTO 488 (ATTO-TEC #AD 488-71) pre-mixed with 40 µM biotin for 30 minutes at RT. The presence of biotin minimises the self-quenching activity of ATTO dye observed with tetravalent Strep-Tactin. Cells were analysed by flow cytometry and the gMFI when cells were incubated with buffer alone instead of Strep-Tactin SpyCatcher was subtracted from all corresponding sample gMFI values. These values were then fitted with the single site binding model, equation below, where Y is the gMFI (AU), Bmax is the maximum specific SpyCatcher binding indicated by gMFI in AU, X is the [Streptactin-SpyCatcher] added (M) and K_D is the [SpyCatcher] that yields 50% maximal binding to CHO cells (M).

$$Y = \frac{Bmax * X}{Kd + X}$$

To convert Y values into the average number of binding sites per ligand cell, the number of binding sites per cell at saturating monovalent/tetravalent Strep-Tactin SpyCatcher concentration calculated in the biotin-4-fluorescein assay was substituted into the equation above as Bmax. Y values were then re-calculated following this adjustment. This method was followed in each independent experiment and then an average value for the K_D and Bmax was used when combining replicates.

Fluorescent recovery after photobleaching

CHO cells (1 x10^5) expressing the three ligand anchors (CD80, CD43 and CD52) were transferred to a 35 mm glass bottom dish one day before imaging. To prepare cells for imaging each dish was washed 3 times with coupling buffer plus 10 % FBS. SpyCatcher-GFP was then added in excess (approximately 10 µM) and left for 10 minutes. Before washing the cells three times in PBS 1 % BSA 10 % FBS. Cells were transferred to the Olympus FV1200 laser scanning microscope with 37 °C chamber for equilibration. The

60X magnification lens was used to locate cells spread over the glass coverslip. A small area of the cell (approximately 10 %) was selected a few control images were taken before a 20 second bleach performed. A time lapse series of images was then taken to track the recovery of the GFP signal.

Time lapse image series were imported into ImageJ for analysis. For each time lapse the bleach area was selected (bleach) along with a control area which was taken to be the rest of the cell contact with the glass (control area) and a negative control area around the outside of the cell (negative). Firstly, the intensity from the negative area was subtracted from the bleach and control area. The bleach area was then divided by the control area for each time frame and these values were normalised to the control image before the bleach was performed. These values were then plotted against time and the equation below used to find the half time for each ligand anchor.

$$Y = Y0 + (Plateau - Y0) * (1 - e^{-K*x})$$

Where Y0 is the value when X (time) is zero, Plateau is the Y value at infinite times and K is the rate constant from which the half time is derived.

The half time value could then be converted into the diffusion coefficient using the equation below (Soumpasis, 1983).

$$Diffusion\ coefficient = 0.224 * r^2 / half\ time$$

Where 0.224 is a constant for a circular bleach area, r is the radius of the bleach area, and the half time is the derived from fitting the one phase association equation to the bleach recovery above.

Ligand turnover

CHO ligand anchor cells were incubated with 15 µM monovalent Strep-Tactin SpyCatcher (or buffer alone) as described above and incubated at 37 °C to match stimulation assays for the time points indicated. Cells were analysed for generic ligand surface expression using ATTO 488 biotin as above and normalised to the geometric fluorescence intensity value at time 0. To calculate the decay, the gMFI values were fitted with the equation below where Y0 is the Y value when X = 0, Plateau is the Y value at which the curve reaches a plateau, X is time in minutes, and K is the rate constant in inverse minutes.

$$Y = (\mathrm{Y0} - \mathrm{Plateau}).e^{-K.X} + \mathrm{Plateau}$$

IL-8 production

CHO ligand anchor cells (2 x 10^5) coupled with either monovalent/tetravalent Strep-Tactin SpyCatcher or buffer alone were mixed with single Strep-tag II tagged receptor and adaptor expressing THP-1 or untransduced THP-1 cells (1 x 10^5) in DMEM 5% FBS, 1 in 100 penicillin/streptomycin, 2 µg mL^{-1} avidin.

Cells were incubated in a 37 °C 10% CO2 containing incubator for 20 hours. Supernatants were harvested and assayed for IL-8 by ELISA following manufacturer's instructions (Thermo Fisher Scientific #88808688).

Conjugation assays

Ligand cells were stained with CellTrace Far Red (Thermo Fisher Scientific #C34564) at a final concentration of 1 µM in PBS at a density of 1 x 10^6 cells per ml. THP-1 receptor cells were stained with CellTrace Violet (Thermo Fisher Scientific #C34557) at a final concentration of 1 µM in PBS for 20 minutes. CHO Ligand cells (4 x 10^5) coupled with either monovalent/tetravalent Strep-Tactin SpyCatcher were mixed with (2 x 10^5) THP-1 cells in PBS 1 % BSA on Ice for 1 hour. Conjugation efficacy was analysed by flow cytometry.

Due to experimental constraints stimulation and conjugation assays were completed on successive days. However, we confirmed that the same result was observed when the stimulation and conjugation assays were performed in parallel on the same day by splitting the cells in half for each assay (Supplementary Figure 2)

Data analysis

For receptor stimulation assays, IL-8 concentrations in negative controls (where CHO cells were pre-incubated with buffer alone instead of Strep-Tactin SpyCatcher) were subtracted from corresponding sample IL-8 concentrations to correct for background levels. Dose-response curves were then fitted with the below equation where Y is the measured cell response (pg mL^{-1}), Bottom and Top are the minimum and maximum cell response respectively (pg mL^{-1}), EC50 is the number of binding sites per cell that yields a half maximal response, X is the number of binding sites per cell and Hill slope relates to the steepness of the curve.

$$Y = Bottom + \frac{(X^{Hillslope})(Top - Bottom)}{(X^{Hillslope} + EC50^{Hillslope})}$$

For conjugate assays the percentage of THP-1 cells forming conjugates was calculated using the formula below. The data was then fit using the same dose response equation above except with X being the percentage of THP-1 cells in conjugates, normalized where indicated.

$$Receptor\ cells\ in\ Conjugates\ (\%) = \frac{Double\ positive\ events}{Receptor\ only\ events + Double\ positive\ events} * 100$$

To plot stimulation as a function of conjugation the average number of binding sites used in the stimulation assay were interpolated from the fit of the conjugation data using the four parameter dose

response model. The IL-8 values from the stimulation were then plotted against the interpolated values of conjugate formation.

For statistical analysis F tests, t tests ANOVA were performed as appropriate and results presented with the following symbols: ns, not significant ; * , $p < 0.05$; **, $p < 0.01$; ***, $p < 0.001$; ****, $p < 0.0001$.

Acknowledgements

We acknowledge Mark Howarth for providing Strep-Tactin, streptavidin, SpyTag and SpyCatcher constructs and for helpful discussions and advice. We thank Marion H Brown and Omer Dushek and their groups for helpful discussion.
This work was supported by a Wellcome Trust Senior Investigator Award (P.A.v.d.M., grant reference: 101799/Z/13/Z) and a Nuffield Medical Fellowship from the Australian Academy of Science (J.G., grant reference: #1016848).

Author Contributions

The study was conceived by PAvdM and JG, the experiments were performed by MIB with reagents prepared by RLP and EMD, the paper was drafted by MIB and PAvdM and finalized by all authors.

Competing interests

PAvdM is a founder of MatchBio Limited.

References

Al-Aghbar MA, Chu Y-S, Chen B-M, Roffler SR. 2018. High-Affinity Ligands Can Trigger T Cell Receptor Signaling Without CD45 Segregation. *Frontiers in immunology* **9**:523. doi:10.3389/fimmu.2018.00713

Angata T, Hayakawa T, Yamanaka M, Varki A, Nakamura M. 2006. Discovery of Siglec-14, a novel sialic acid receptor undergoing concerted evolution with Siglec-5 in primates. *FASEB J* **20**:1964–1973. doi:10.1096/fj.06-5800com

Bakalar MH, Joffe AM, Schmid EM, Son S, Podolski M, Fletcher DA. 2018. Size-Dependent Segregation Controls Macrophage Phagocytosis of Antibody-Opsonized Targets. *Cell* **174**:131–142. doi:10.1016/j.cell.2018.05.059

Barclay AN, Brown MH, Law SKA, McKnight AJ, Tomlinson MG, van der Merwe PA. 1997. The Leucocyte Antigen Factsbook, 2nd ed, Academic Press. Academic Press.

Boniface JJ, Boniface J, Rabinowitz JD, Rabinowitz J, Wulfing C, Hampl J, Reich Z, Altman J, Altman JD, Kantor RM, Kantor R, Beeson C, McConnell HM, McConnell H, Davis M M, Davis Mark M. 1998. Initiation of signal transduction through the T cell receptor requires the multivalent engagement of peptide/MHC ligands [corrected]. *IMMUNITY* **9**:459–466.

Burroughs NJ, Lazic Z, van der Merwe PA. 2006. Ligand detection and discrimination by spatial relocalization: A kinase-phosphatase segregation model of TCR activation. *Biophysical journal* **91**:1619–1629. doi:10.1529/biophysj.105.080044

Chang VT, Fernandes RA, Ganzinger KA, Lee SF, Siebold C, McColl J, Jönsson P, Palayret M, Harlos K, Coles CH, Jones EY, Lui Y, Huang E, Gilbert RJC, Klenerman D, Aricescu AR, Davis SJ. 2016. Initiation of T cell signaling by CD45 segregation at “close contacts.” *Nat Immunol* **17**:574–582. doi:10.1038/ni.3392

Chen B-M, Al-Aghbar MA, Lee Chien-Hsin, Chang T-C, Su Y-C, Li Y-C, Chang S-E, Chen C-C, Chung T-H, Liao Y-C, Lee Chau-Hwang, Roffler SR. 2017. The Affinity of Elongated Membrane-Tethered Ligands Determines Potency of T Cell Receptor Triggering. *Front Immunol* **8**:793. doi:10.3389/fimmu.2017.00793

Chen KY, Jenkins E, Körbel M, Ponjavic A, Lippert AH, Santos AM, Ashman N, O’Brien-Ball C, McBride J, Klenerman D, Davis SJ. 2021. Trapping or slowing the diffusion of T cell receptors at close contacts initiates T cell signaling. *Proc National Acad Sci* **118**:e2024250118. doi:10.1073/pnas.2024250118

Choudhuri K, Wiseman D, Brown MH, Gould K, van der Merwe PA. 2005. T-cell receptor triggering is critically dependent on the dimensions of its peptide-MHC ligand. *Nature* **436**:578–582. doi:10.1038/nature03843

Cochran JR, Cameron TO, Stern LJ. 2000. The Relationship of MHC-Peptide Binding and T Cell Activation Probed Using Chemically Defined MHC Class II Oligomers. *Immunity* **12**:241–250. doi:10.1016/s1074-7613(00)80177-6

Cordoba S-P, Choudhuri K, Zhang H, Bridge M, Basat AB, Dustin ML, van der Merwe PA. 2013. The large ectodomains of CD45 and CD148 regulate their segregation from and inhibition of ligated T-cell receptor. *Blood* **121**:4295–4302. doi:10.1182/blood-2012-07-442251

Cornish AL, Freeman S, Forbes G, Ni J, Zhang M, Cepeda M, Gentz R, Augustus M, Carter KC, Crocker PR. 1998. Characterization of Siglec-5, a Novel Glycoprotein Expressed on Myeloid Cells Related to CD33. *Blood* **92**:2123–2132. doi:10.1182/blood.v92.6.2123.418k20_2123_2132

Crocker PR, Paulson JC, Varki A. 2007. Siglecs and their roles in the immune system. *Nature Reviews Immunology* **7**:255–266. doi:10.1038/nri2056

Davis SJ, van der Merwe PA. 2006. The kinetic-segregation model: TCR triggering and beyond. *Nature Immunology* **7**:803–809. doi:10.1038/ni1369

Davis SJ, van der Merwe PA. 1996. The structure and ligand interactions of CD2: implications for T-cell function. *Immunol Today* **17**:177–187. doi:10.1016/0167-5699(96)80617-7

Denham EM, Barton MI, Black SM, Bridge MJ, Wet B de, Paterson RL, van der Merwe PA, Goyette J. 2019. A generic cell surface ligand system for studying cell–cell recognition. *Plos Biol* **17**:e3000549. doi:10.1371/journal.pbio.3000549

Dushek O, Goyette J, van der Merwe PA. 2012. Non-catalytic tyrosine-phosphorylated receptors. *Immunological Reviews* **250**:258–276. doi:10.1111/imr.12008

Ford JW, McVicar DW. 2009. TREM and TREM-like receptors in inflammation and disease. *Current opinion in immunology* **21**:38–46. doi:10.1016/j.coi.2009.01.009

Göhring J, Kellner F, Schrangl L, Platzer R, Klotzsch E, Stockinger H, Huppa JB, Schütz GJ. 2021. Temporal analysis of T-cell receptor-imposed forces via quantitative single molecule FRET measurements. *Nat Commun* **12**:2502. doi:10.1038/s41467-021-22775-z

Goodridge HS, Reyes CN, Becker CA, Katsumoto TR, Ma J, Wolf AJ, Bose N, Chan ASH, Magee AS, Danielson ME, Weiss A, Vasilakos JP, Underhill DM. 2011. Activation of the innate immune receptor Dectin-1 upon formation of a 'phagocytic synapse.' *Nature* **472**:471–475. doi:10.1038/nature10071

Goyette J, Nieves DJ, Ma Y, Gaus K. 2019. How does T cell receptor clustering impact on signal transduction? *Journal of cell science* **132**:jcs226423. doi:10.1242/jcs.226423

James JR, Vale RD. 2012. Biophysical mechanism of T-cell receptor triggering in a reconstituted system. *Nature* **487**:64–69. doi:10.1038/nature11220

Jenkins E, Körbel M, O'Brien-Ball C, McColl J, Chen KY, Kotowski M, Humphrey J, Lippert AH, Brouwer H, Santos AM, Lee SF, Davis SJ, Klenerman D. 2023. Antigen discrimination by T cells relies on size-constrained microvillar contact. *Nat Commun* **14**:1611. doi:10.1038/s41467-023-36855-9

June CH, Sadelain M. 2018. Chimeric Antigen Receptor Therapy. *New Engl J Med* **379**:64–73. doi:10.1056/nejmra1706169

Jung Y, Wen L, Altman A, Ley K. 2021. CD45 pre-exclusion from the tips of T cell microvilli prior to antigen recognition. *Nat Commun* **12**:3872. doi:10.1038/s41467-021-23792-8

Köhler K, Xiong S, Brzostek J, Mehrabi M, Eissmann P, Harrison A, Cordoba S-P, Oddos S, Miloserdov V, Gould K, Burroughs NJ, van der Merwe PA, Davis DM. 2010. Matched sizes of activating and inhibitory receptor/ligand pairs are required for optimal signal integration by human natural killer cells. *PLOS One* **5**:e15374. doi:10.1371/journal.pone.0015374

Labanieh L, Mackall CL. 2023. CAR immune cells: design principles, resistance and the next generation. *Nature* **614**:635–648. doi:10.1038/s41586-023-05707-3

Lanier LL. 2008. DAP10- and DAP12-associated receptors in innate immunity. *Immunological reviews* **227**:150–160. doi:10.1111/j.1600-065x.2008.00720.x

Li Y-C, Chen B-M, Wu P-C, Cheng T-L, Kao L-S, Tao M-H, Lieber A, Roffler SR. 2010. Cutting Edge: Mechanical Forces Acting on T Cells Immobilized via the TCR Complex Can Trigger TCR Signaling. *J Immunol* **184**:5959–5963. doi:10.4049/jimmunol.0900775

Lim H-S, Cordoba S-P, Dushek O, Goyette J, Taylor A, Rudd CE, van der Merwe PA. 2015. Costimulation of IL-2 Production through CD28 Is Dependent on the Size of Its Ligand. *Journal of immunology (Baltimore, Md : 1950)* **195**:5432–5439. doi:10.4049/jimmunol.1500707

Locksley RM, Killeen N, Lenardo MJ. 2001. The TNF and TNF Receptor Superfamilies Integrating Mammalian Biology. *Cell* **104**:487–501. doi:10.1016/s0092-8674(01)00237-9

Ma Z, Janmey PA, Finkel TH. 2008. The receptor deformation model of TCR triggering. *The FASEB Journal* **22**:1002–1008. doi:10.1096/fj.07-9331hyp

van der Merwe PA, Barclay AN. 1994. Transient intercellular adhesion: the importance of weak protein-protein interactions. *Trends Biochem Sci* **19**:354–358. doi:10.1016/0968-0004(94)90109-0

van der Merwe PA, Davis SJ, Shaw AS, Dustin ML. 2000. Cytoskeletal polarization and redistribution of cell-surface molecules during T cell antigen recognition. *Semin Immunol* **12**:5–21. doi:10.1006/smim.2000.0203

Milstein O, Tseng S-Y, Starr T, Llodra J, Nans A, Liu M, Wild MK, van der Merwe PA, Stokes DL, Reisner Y, Dustin ML. 2008. Nanoscale Increases in CD2-CD48-mediated Intermembrane Spacing Decrease Adhesion and Reorganize the Immunological Synapse*. *J Biol Chem* **283**:34414–34422. doi:10.1074/jbc.m804756200

O'Shea JJ, McVicar DW, Bailey TL, Burns C, Smyth MJ. 1992. Activation of human peripheral blood T lymphocytes by pharmacological induction of protein-tyrosine phosphorylation. *Proceedings of the National Academy of Sciences of the United States of America* **89**:10306–10310.

Parodi M, Favoreel H, Candiano G, Gaggero S, Sivori S, Mingari MC, Moretta L, Vitale M, Cantoni C. 2019. NKp44-NKp44 Ligand Interactions in the Regulation of Natural Killer Cells and Other Innate Lymphoid Cells in Humans. *Front Immunol* **10**:719. doi:10.3389/fimmu.2019.00719

Patel A, Andre V, Eguiguren SB, Barton MI, Denham EM, Pettmann J, Morch AM, Kutuzov M, Siller-Farfan JA, Dustin ML, van der Merwe PA, Dushek O. 2023. Using CombiCells, a platform enabling titration and combinatorial display of cell surface ligands, to investigate the sensitivity and costimulatory requirements of TCRs and CARs. doi:10.1101/2023.06.15.545075

Razvag Y, Neve-Oz Y, Sajman J, Reches M, Sherman E. 2018. Nanoscale kinetic segregation of TCR and CD45 in engaged microvilli facilitates early T cell activation. *Nature Communications* **9**:732. doi:10.1038/s41467-018-03127-w

Sadelain M. 2016. Chimeric antigen receptors: driving immunology towards synthetic biology. *Current opinion in immunology* **41**:68–76. doi:10.1016/j.coi.2016.06.004

Schamel WW, Alarcón B, Minguet S. 2019. The TCR is an allosterically regulated macromolecular machinery changing its conformation while working. *Immunological reviews* **291**:8–25. doi:10.1111/imr.12788

Schmid EM, Bakalar MH, Choudhuri K, Weichsel J, Ann HS, Geissler PL, Dustin ML, Fletcher DA. 2016. Size-dependent protein segregation at membrane interfaces. *Nature Physics*. doi:10.1038/nphys3678

Secrist JP, Burns LA, Karnitz L, Koretzky GA, Abraham RT. 1993. Stimulatory effects of the protein tyrosine phosphatase inhibitor, pervanadate, on T-cell activation events. *Journal of Biological Chemistry* **268**:5886–5893.

Sharma P, Allison JP. 2015. The future of immune checkpoint therapy. *Science* **348**:56–61. doi:10.1126/science.aaa8172

Shilts J, Severin Y, Galaway F, Müller-Sienerth N, Chong Z-S, Pritchard S, Teichmann S, Vento-Tormo R, Snijder B, Wright GJ. 2022. A physical wiring diagram for the human immune system. *Nature* **608**:397–404. doi:10.1038/s41586-022-05028-x

Springer TA. 1990. Adhesion receptors of the immune system. *Nature* **346**:425–434. doi:10.1038/346425a0

Stinchcombe JC, Asano Y, Kaufman CJG, Böhlig K, Peddie CJ, Collinson LM, Nadler A, Griffiths GM. 2023. Ectocytosis renders T cell receptor signaling self-limiting at the immune synapse. *Science* **380**:818–823. doi:10.1126/science.abp8933

Ullrich A, Schlessinger J. 1990. Signal transduction by receptors with tyrosine kinase activity. *Cell* **61**:203–212. doi:10.1016/0092-8674(90)90801-k

Varma R, Campi G, Yokosuka T, Saito T, Dustin ML. 2006. T Cell Receptor-Proximal Signals Are Sustained in Peripheral Microclusters and Terminated in the Central Supramolecular Activation Cluster. *Immunity* **25**:117–127. doi:10.1016/j.immuni.2006.04.010

Wild MK, Cambiaggi A, Brown MH, Davies EA, Ohno H, Saito T, van der Merwe PA. 1999. Dependence of T Cell Antigen Recognition on the Dimensions of an Accessory Receptor–Ligand Complex. *J Exp Medicine* **190**:31–42. doi:10.1084/jem.190.1.31

Wilhelm KB, Morita S, McAffee DB, Kim S, O'Dair MK, Groves JT. 2021. Height, but not binding epitope, affects the potency of synthetic TCR agonists. *Biophys J* **120**:3869–3880. doi:10.1016/j.bpj.2021.08.027

Wu H, Kwong PD, Hendrickson WA. 1997. Dimeric association and segmental variability in the structure of human CD4. *Nature* **387**:527–530. doi:10.1038/387527a0

Xiao Q, Zhang X, Tu L, Cao J, Hinrichs CS, Su X. 2022. Size-dependent activation of CAR-T cells. *Sci Immunol* **7**:eabl3995. doi:10.1126/sciimmunol.abl3995

Zhu C, Chen W, Lou J, Rittase W, Li K. 2019. Mechanosensing through immunoreceptors. *Nat Immunol* **20**:1269–1278. doi:10.1038/s41590-019-0491-1

Figure legends

Figure 1 Testing the effect of increasing ligand length on NTR activation

(A) Schematic depiction of the components of the generic ligand system used to test the effect of increasing ligand length and valency. (B) Representative flow cytometry data from a conjugation assay between SIRPβ1 expressing THP1 receptor cells and CHO cells expressing short ligands coupled with the indicated concentration of monovalent Strep-Tactin SpyCatcher. Receptor and ligand cells were stained with CellTrace Violet and Far Red, respectively, and events in the upper right quadrant were presumed to be conjugates. (C) Conjugation of (left panel) and IL-8 secretion by (middle panel) SIRPβ1 expressing THP1 cells incubated with CHO cells expressing the indicated number of short or long monovalent ligands, measured as described in the Materials and Methods using parameters determined in sFigure 1. IL-8 secretion is plotted against conjugation in the right panel. These are representative results from three independent experiments, which are combined in Figure 2A for statistical analysis. Due to experimental constraints the stimulation and conjugation assays in this (and subsequent) experiment(s) were performed on successive days. The same result was obtained when performed on the same day (sFigure 2).

Figure 2: The effect of NTR ligand length on activation via four NTRs.

THP-1 cells expressing (A) SIRPβ1, (B) Siglec 14, (C) NKp44 or (D) TREM-1 with N-terminal StrepTagII peptides were incubated with CHO cells expressing the indicated numbers of short or long generic ligand binding sites and conjugate formation (left panel) and IL-8 release (middle panel) measured. Ligand binding sites were determined as described in the Materials and Methods using parameters determined in sFigure 1. The IL-8 release versus conjugation level is plotted in the right panels. The data from three biological replicates (including one SIRPβ1 replicate shown in Figure 1) are plotted with the data normalised to the level of conjugation or stimulation achieved with the short ligand within each replicate. The data were fitted as described in the Materials and Methods and an F test was used to test the significance of differences between the fits.

Figure 3: Effect of ligand anchor on SIRPβ1 stimulation

(A) Schematic depiction of the components of the generic ligand system used to test the effect of varying the ligand anchor. (B) The diffusion coefficients of the different ligand anchors were measured by FRAP after coupling GFP-Spycatcher. The mean and SD from three independent experiments were compared by ANOVA. (C) THP-1 cells expressing SIRPβ1 with an N-terminal StrepTagII peptide were incubated with CHO cells expressing the indicated number of ligand binding sites and conjugate formation (left panel) and IL-8 release (right panel) measured. Ligand binding sites were determined as

described in the Materials and Methods using parameters determined in sFigure 4. The IL-8 release versus conjugation level is plotted in the right panel. The data from three biological replicates are plotted with the data normalised to the level of conjugation or stimulation achieved with the CD52 ligand anchor within each replicate. These data were fitted as described in the Materials and Methods and an F test was used to test the significance of differences between the fits.

Figure 4: Effect of ligand valency on NTR stimulation.

THP-1 cells expressing (A) SIRPβ1, (B) Siglec 14, (C) NKp44 or (D) TREM-1 with N-terminal StrepTagII peptides were incubated with CHO cells expressing the indicated numbers of monovalent or tetravalent short generic ligand binding sites and conjugate formation (left panel) and IL-8 release (middle panel) measured. Ligand binding sites were determined as described in the Materials and Methods using parameters determined in sFigure 6. The IL-8 release versus conjugation level is plotted in the right panels. The data from three biological replicates are plotted with the data normalised to the level of conjugation or stimulation achieved with the short tetravalent ligand within each replicate. These data were fitted as described in the Materials and Methods and an F test was used to test the significance of differences between the fits.

Figure 5: The effect of NTR ligand length on activation by tetravalent ligands

THP-1 cells expressing (A) SIRPβ1, (B) Siglec 14, (C) NKp44 or (D) TREM-1 with N-terminal StrepTagII peptides were incubated with CHO cells expressing the indicated numbers of short or long tetravalent ligand binding sites and conjugate formation (left panel) and IL-8 release (middle panel) measured. Ligand binding sites were determined as described in the Materials and Methods using parameters determined in sFigure 9. The IL-8 release versus conjugation level is plotted in the right panels. The data from three biological replicates are plotted with the data normalised to the level of conjugation or stimulation achieved with the short tetravalent ligand within each replicate. These data were fitted as described in the Materials and Methods and an F test was used to test the significance of differences between the fits.

Supplementay Figure legends

sFigure 1. Measuring the K_D and maximum number of binding sites on CHO cell expressing short and long CD80 ligand anchors

(A) Short or long CD80 ligand CHO cells were incubated with the indicated concentration of monovalent StrepTactin SpyCatcher before labelling with biotin Atto 488 followed by flow cytometry. A one site simple binding model was fitted to the data (lines) to determine the K_D. (B) The mean and SD of K_D values from six independent experiments were compared using a t test. (C) Short or long CD80 ligand CHO cells or control (empty) CHO cells were incubated with a saturating concentration (15 μM) of monovalent StrepTactin SpyCatcher before mixing with the indicated concentration of biotin-4-fluorescein and the unquenched fluorescence in the media measured after binding. (D) The mean and SD of the maximum number of binding sites per cell from six independent experiments were compared using a t test.

sFigure 2. Testing the effect of increasing ligand length on NTR activation

Repeat of experiment Figure 1 with both conjugation and stimulation assays performed on the same day with the same cells split. THP-1 cells expressing SIRPβ1 were incubated with CHO cells expressing the indicated numbers of short or long generic ligand binding sites and conjugate formation (A) and IL-8 release (B) measured. Ligand binding sites were determined as described in the Materials and Methods using parameters determined in sFigure 1. The IL-8 release versus conjugation level is plotted in (C).

sFigure 3. The effect of NTR length on activation.

The data from Figure 2 has been reanalysed to enable comparison between NTRs. THP-1 cells expressing the indicated NTR with N-terminal StrepTagII peptides were incubated with CHO cells expressing the indicated numbers of short (A) or long (B) generic ligand binding sites and conjugate formation (left panel) and IL-8 release (middle panel) measured. The IL-8 release versus conjugation level is plotted in the right panels. The data were fitted as described in the Materials and Methods and an F test was used to test the significance of differences between the fits.

sFigure 4. K_D and maximum generic binding sites on CHO cell expressing different ligand anchors

(A) Mean and SD of K_D values determined as in sFigure 1 from nine independent experiments (B) Mean and SD of maximum number of binding sites determined as in sFigures 1 from six independent experiments. To enable comparison to monovalent sites the tetravalent values divided by four, labelled (/4), were also plotted.

sFigure 5. Turnover of ligand anchor at the cell surface.

(A-C) Monovalent StrepTactin SpyCatcher was coupled to CHO cells expressing the indicated ligand anchor and cells incubated at 37 C for the indicated times. Cells were stained with biotin ATTO 488 and analysed by flow cytometry to assess the level of the cell surface StrepTactin. The graphs show the relative level of ligand expression with the maximum normalised to time zero. The data is a representative of three biological replicates and was fit with an exponential one phase decay model. (D) The mean and SD of the half-time for loss from the cell surface for three biological replicates were compared by ANOVA.

sFigure 6. Measuring the K_D and maximum number of binding sites on CHO cell presenting monovalent or tetravalent StrepTactin SpyCatcher

(A) Short CD80 ligand CHO cells were incubated with the indicated concentration of monovalent or tetravalent StrepTactin SpyCatcher before labelling with biotin Atto 488 followed by flow cytometry. A one site simple binding model was fitted to the data (lines) to determine the K_D. (B) The mean and SD of K_D values from eight independent experiments were compared using a t test. (C) Short CD80 ligand CHO cells or control (empty) CHO cells were incubated with a saturating concentration monovalent (10 μM) or tetravalent (10 μM) StrepTactin SpyCatcher before mixing with the indicated concentration of biotin-4-fluorescein and the unquenched florescence in the media measured after binding. (D) The mean and SD of the maximum number of binding sites per cell from five independent experiments were compared by ANOVA. To enable comparison to monovalent sites the tetravalent values divided by four were also plotted.

sFigure 7. Effect of anchor on NTR stimulation by multivalent ligand

THP-1 cells expressing (A) SIRPβ1, (B) Siglec 14, (C) NKp44 or (D) TREM-1 with an N-terminal StrepTagII peptide were incubated with CHO cells expressing the indicated number of monovalent or multivalent ligand binding sites with the indicated ligand anchors and IL-8 release measured. Ligand binding sites were determined as described in the Materials and Methods using parameters determined in sFigure 4. The data from three biological replicates are plotted with the data normalised to the level of stimulation achieved with the CD80 ligand coupled with tetravalent ligand within each replicate. These data were fitted as described in the Material and Methods and an F test was used to test the significance of differences between the fits.

sFigure 8. Effect of anchor on SIRPβ1 stimulation by multivalent ligand

THP-1 cells expressing SIRPβ1 with an N-terminal StrepTagII peptide were incubated with CHO cells expressing the indicated number of ligand binding sites presented on the indicated ligand and conjugate

formation (left panel) and IL-8 release (middle panel) were measured. Ligand binding sites were determined as described in the Materials and Methods using parameters determined in sFigure 4. The IL-8 release versus conjugation level is plotted in the right panel. The data from three biological replicates are plotted with the data normalised to the level of conjugation or stimulation achieved with the tetravalent ligand within each replicate. These data were fitted as described in the Material and Methods and an F test was used to test the significance of differences between the fits.

sFigure 9. Measuring the K_D and maximum number of binding sites on CHO cell presenting tetravalent StrepTactin SpyCatcher coupled to short versus long ligand anchors

(A) Short or long CD80 ligand CHO cells were incubated with the indicated concentration of tetravalent StrepTactin SpyCatcher before labelling with biotin Atto 488 followed by flow cytometry. A one site simple binding model was fitted to the data (lines) to determine the K_D. (B) The mean and SD of K_D values from six independent experiments were compared using a t test. (C) Short or long CD80 ligand CHO cells or control (empty) CHO cells were incubated with a saturating concentration (10 μM) of tetravalent StrepTactin SpyCatcher before mixing with the indicated concentration of biotin-4-fluorescein and the unquenched florescence in the media measured after binding. (D) The mean and SD of the maximum number of binding sites per cell from six independent experiments were compared using a t test.

Figure 1

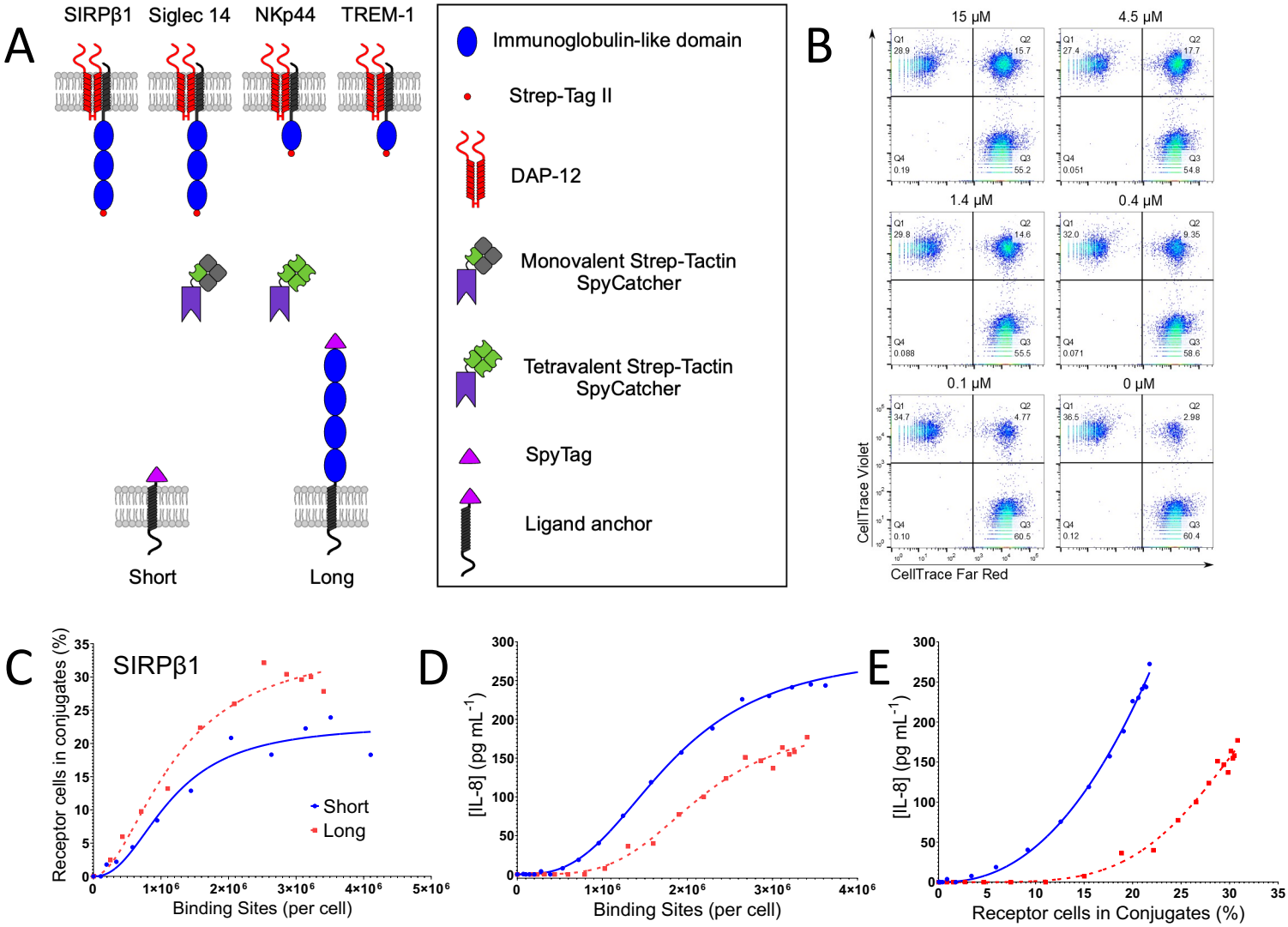
A
SIRPβ1
Siglec 14
NKp44
TREM-1
Short
Long
Immunoglobulin-like domain
Strep-Tag II
DAP-12
Monovalent Strep-Tactin SpyCatcher
Tetravalent Strep-Tactin SpyCatcher
SpyTag
Ligand anchor
B
15 μM
4.5 μM
1.4 μM
0.4 μM
0.1 μM
0 μM
CellTrace Violet
CellTrace Far Red
C
SIRPβ1
Receptor cells in conjugates (%)
Binding Sites (per cell)
Short
Long
D
[IL-8] (pg mL-1)
Binding Sites (per cell)
E
[IL-8] (pg mL-1)
Receptor cells in Conjugates (%)

Figure 2

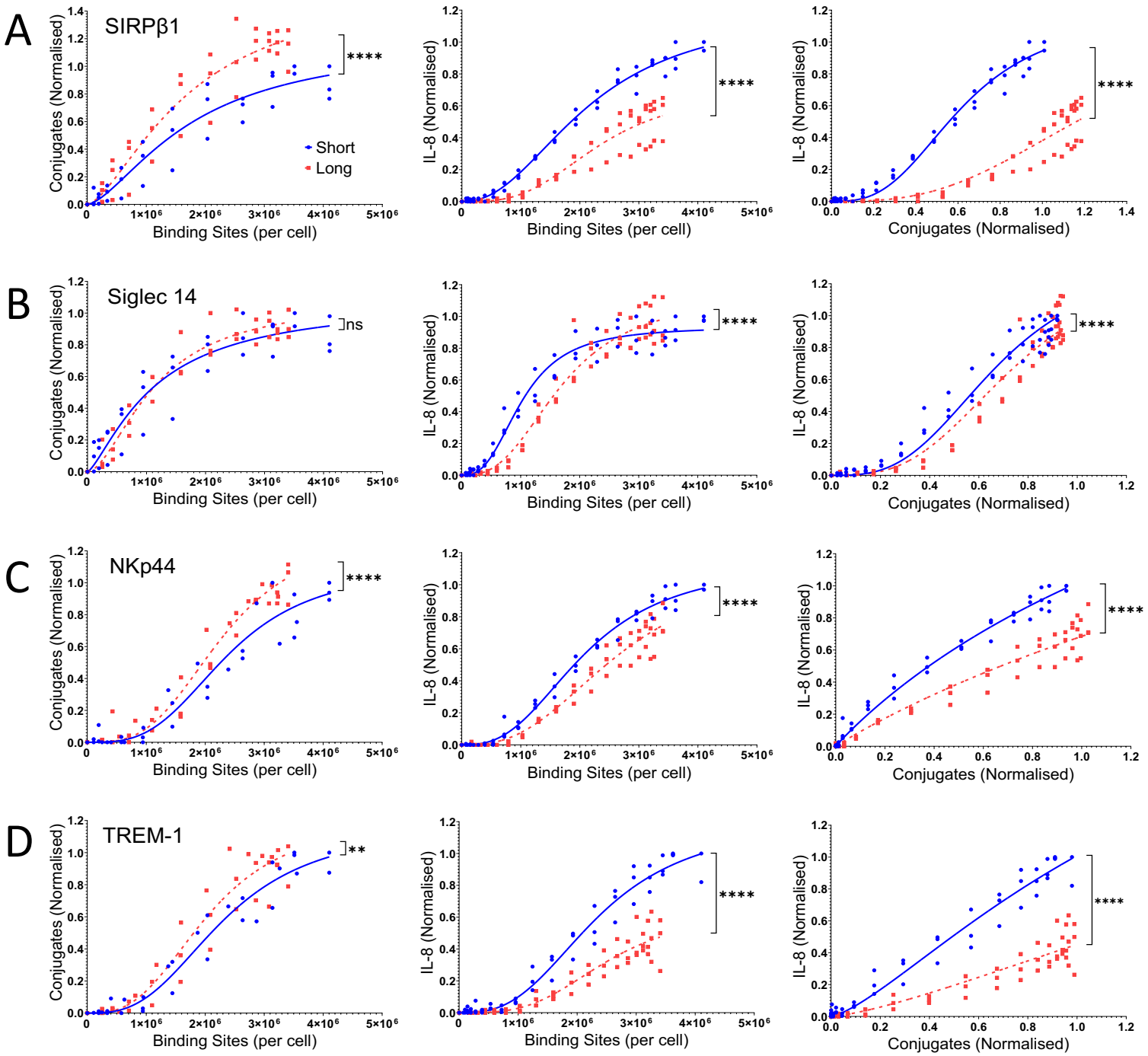
A
SIRPβ1
Short
Long
****
Conjugates (Normalised)
Binding Sites (per cell)
IL-8 (Normalised)
Conjugates (Normalised)
B
Siglec 14
ns
C
NKp44
D
TREM-1
**

Figure 3

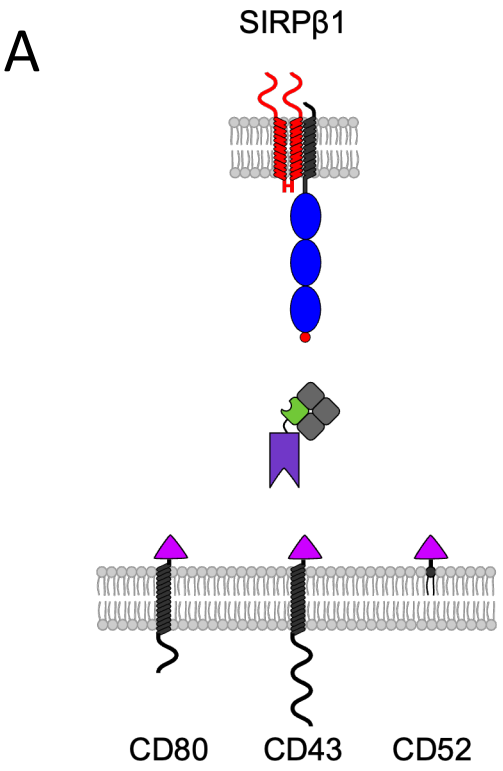

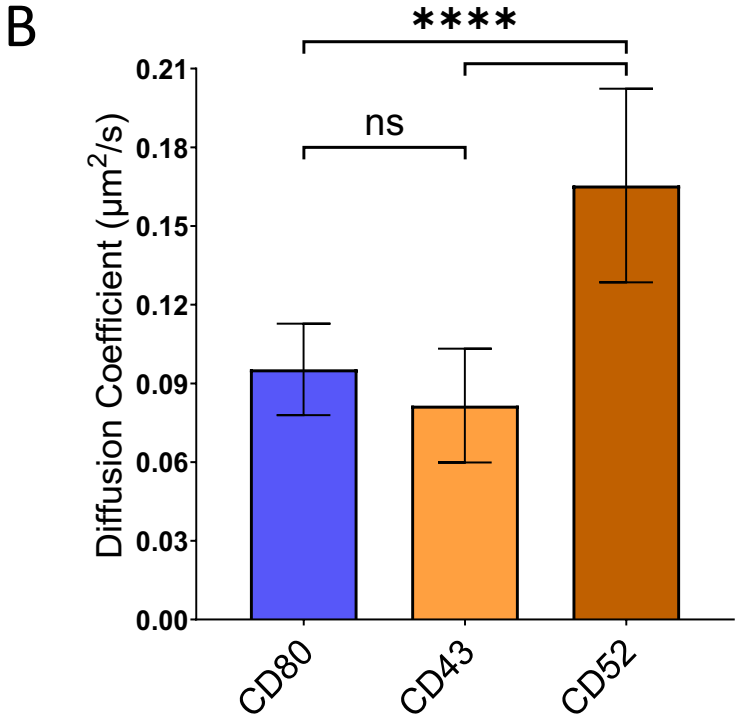

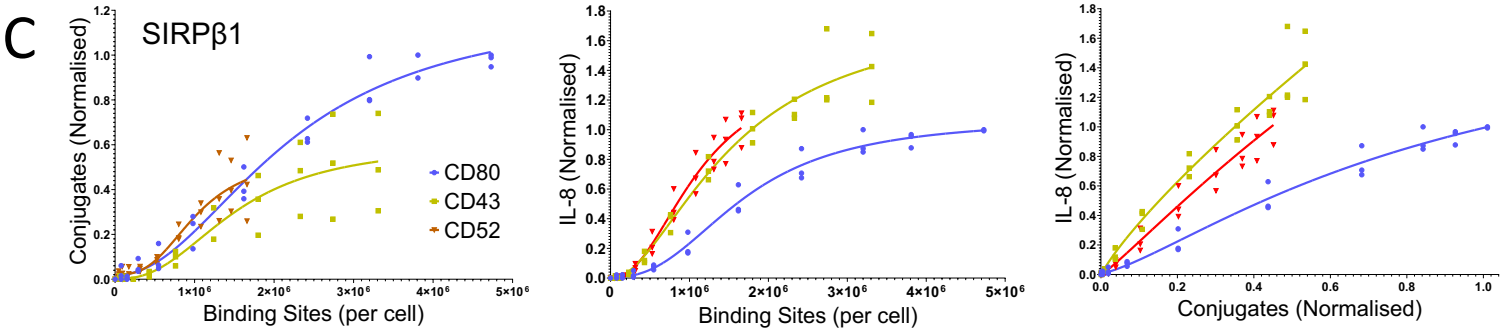

F Test	P value
CD80 vs CD43	<0.0001
CD80 vs CD52	0.5101
CD43 vs CD52	0.1139

F Test	P value
CD80 vs CD43	<0.0001
CD80 vs CD52	<0.0001
CD43 vs CD52	0.4320

F Test	P value
CD80 vs CD43	<0.0001
CD80 vs CD52	<0.0001
CD43 vs CD52	<0.0001

Figure 4

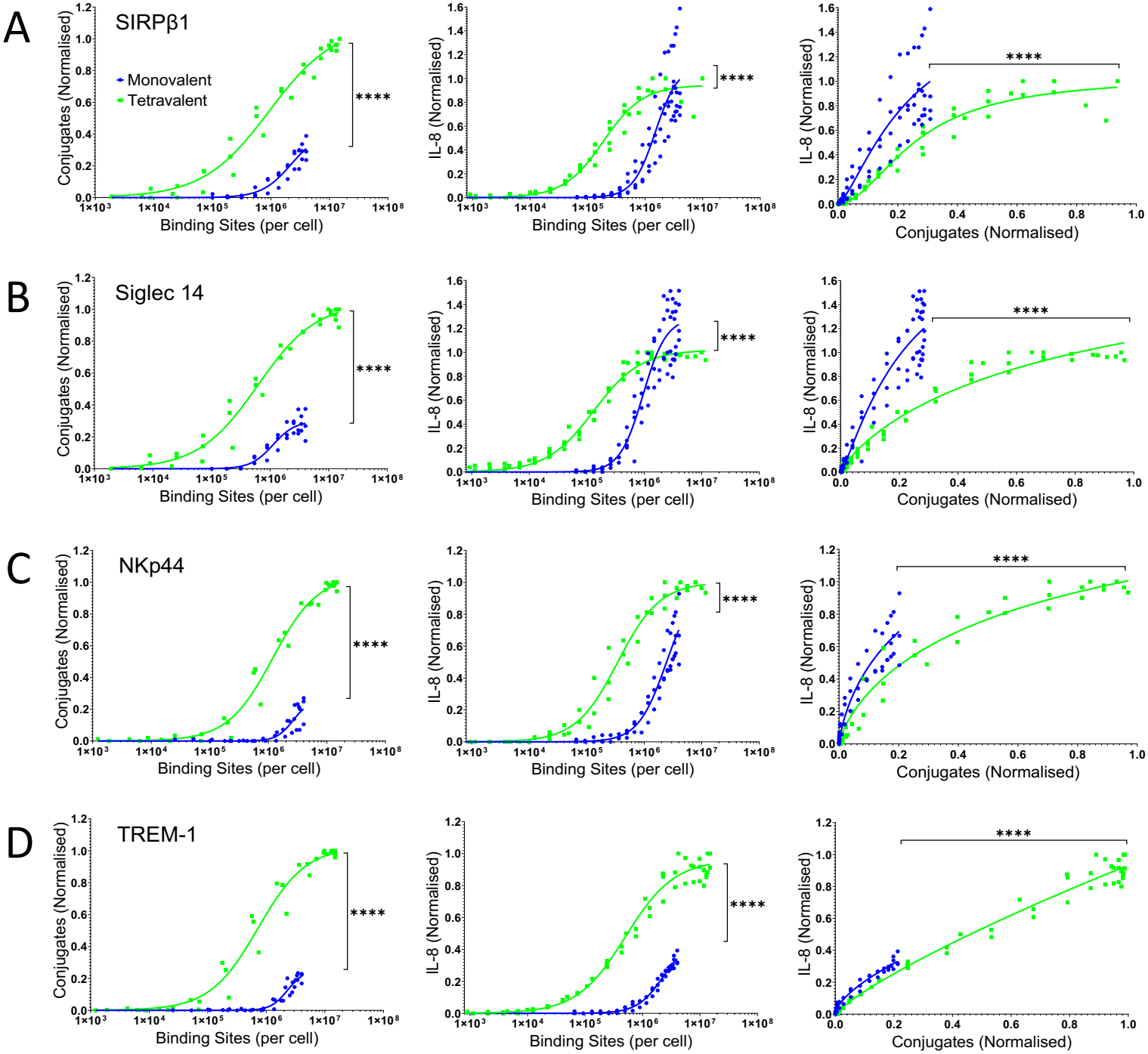
A
SIRPβ1
Monovalent
Tetravalent
Conjugates (Normalised)
Binding Sites (per cell)
IL-8 (Normalised)
Conjugates (Normalised)
****
B
Siglec 14
C
NKp44
D
TREM-1

Figure 5

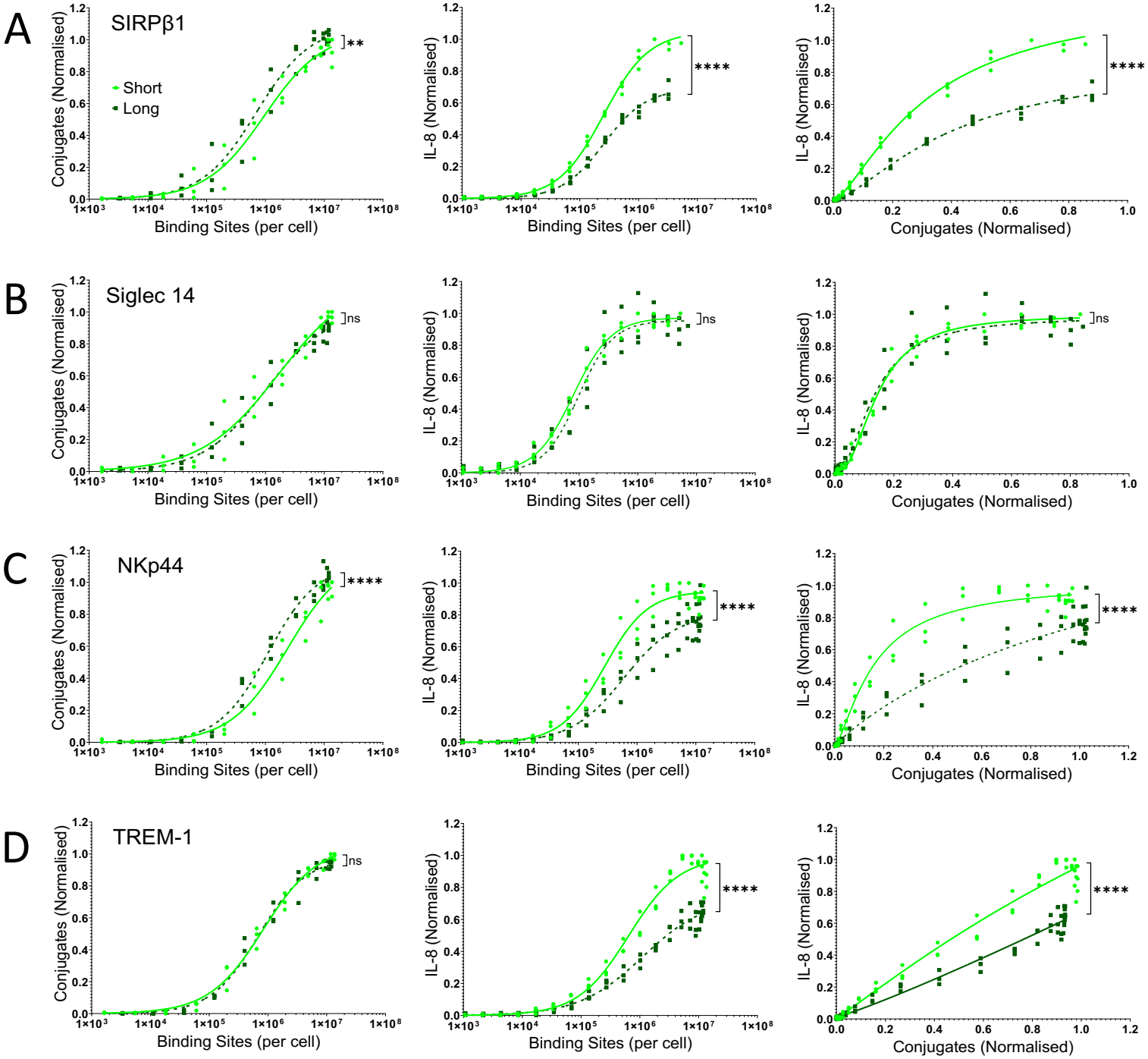
A
SIRPβ1
Short
Long
Conjugates (Normalised)
Binding Sites (per cell)
**
IL-8 (Normalised)
Binding Sites (per cell)
****
IL-8 (Normalised)
Conjugates (Normalised)
****
B
Siglec 14
Conjugates (Normalised)
Binding Sites (per cell)
ns
IL-8 (Normalised)
Binding Sites (per cell)
ns
IL-8 (Normalised)
Conjugates (Normalised)
ns
C
NKp44
Conjugates (Normalised)
Binding Sites (per cell)
****
IL-8 (Normalised)
Binding Sites (per cell)
****
IL-8 (Normalised)
Conjugates (Normalised)
****
D
TREM-1
Conjugates (Normalised)
Binding Sites (per cell)
ns
IL-8 (Normalised)
Binding Sites (per cell)
****
IL-8 (Normalised)
Conjugates (Normalised)
****

sFigure 1

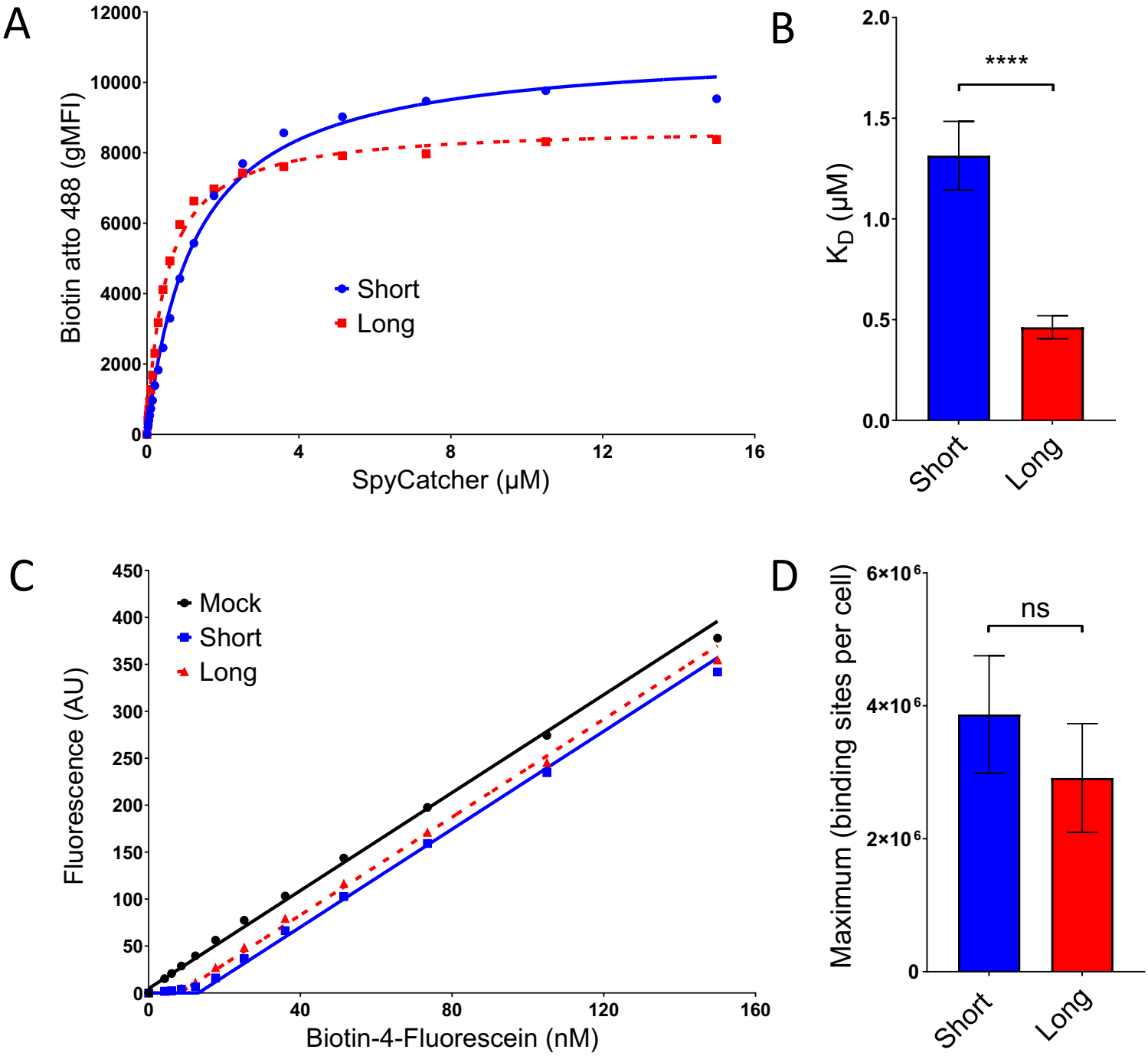
A
Biotin atto 488 (gMFI)
12000
10000
8000
6000
4000
2000
0
0
4
8
12
16
SpyCatcher (μM)
Short
Long
B
K_D (μM)
2.0
1.5
1.0
0.5
0.0
****
Short
Long
C
Fluorescence (AU)
450
400
350
300
250
200
150
100
50
0
0
40
80
120
160
Biotin-4-Fluorescein (nM)
Mock
Short
Long
D
Maximum (binding sites per cell)
6×10^6
4×10^6
2×10^6
0
ns
Short
Long

sFigure 2

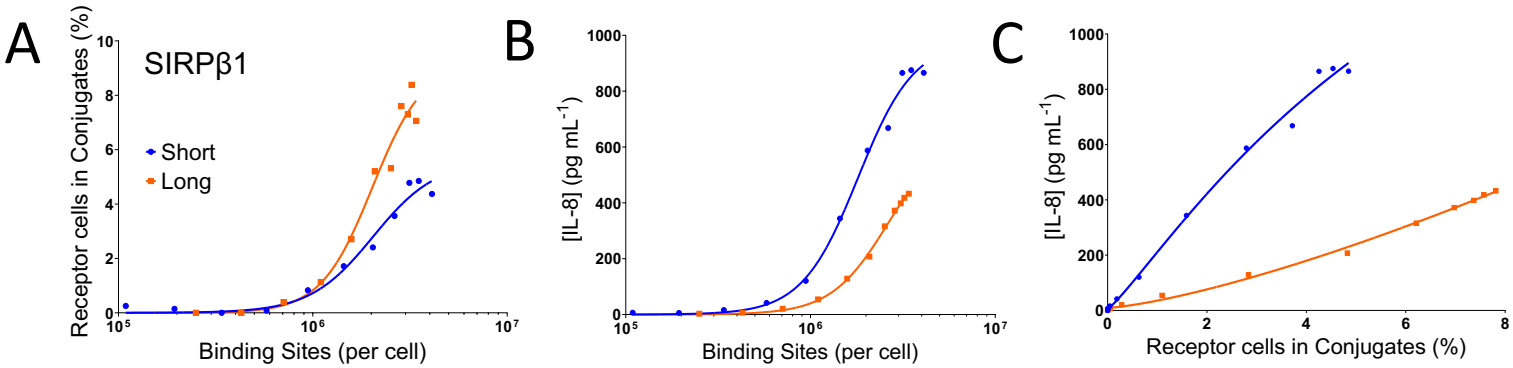
A
SIRPβ1
Short
Long
Receptor cells in Conjugates (%)
Binding Sites (per cell)
B
[IL-8] (pg mL-1)
Binding Sites (per cell)
C
[IL-8] (pg mL-1)
Receptor cells in Conjugates (%)

sFigure 3

A

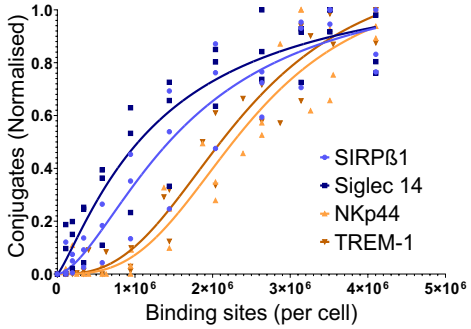

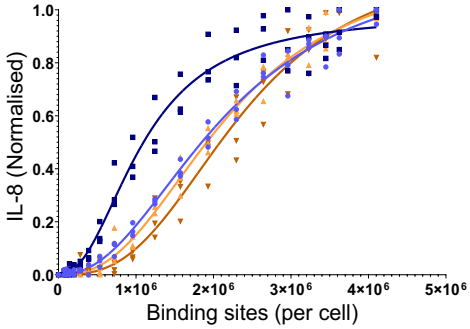

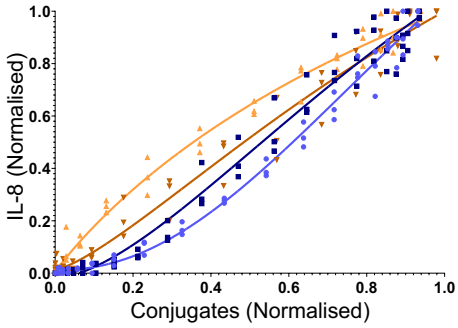

F Test	P value
SIRPß1 vs Siglec 14	0.0443
SIRPß1 vs NKp44	<0.0001
SIRPß1 vs TREM-1	<0.0001
Siglec 14 vs NKp44	<0.0001
Siglec 14 vs TREM-1	<0.0001
NKp44 vs TREM-1	0.4043

F Test	P value
SIRPß1 vs Siglec 14	<0.0001
SIRPß1 vs NKp44	0.0699
SIRPß1 vs TREM-1	<0.0001
Siglec 14 vs NKp44	<0.0001
Siglec 14 vs TREM-1	<0.0001
NKp44 vs TREM-1	0.0055

F Test	P value
SIRPß1 vs Siglec 14	<0.0001
SIRPß1 vs NKp44	<0.0001
SIRPß1 vs TREM-1	<0.0001
Siglec 14 vs NKp44	<0.0001
Siglec 14 vs TREM-1	<0.0001
NKp44 vs TREM-1	<0.0001

B

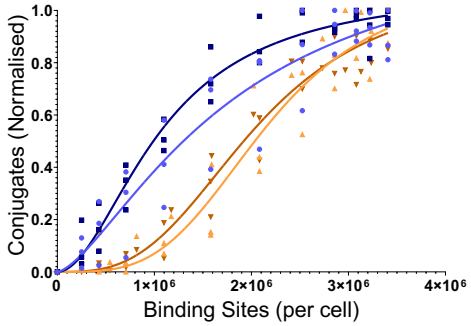

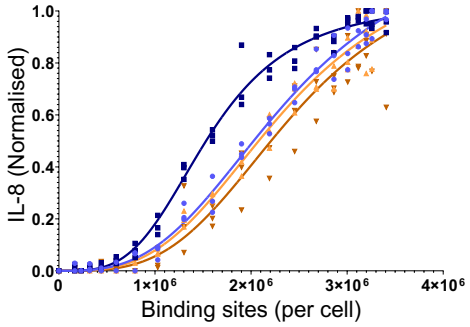

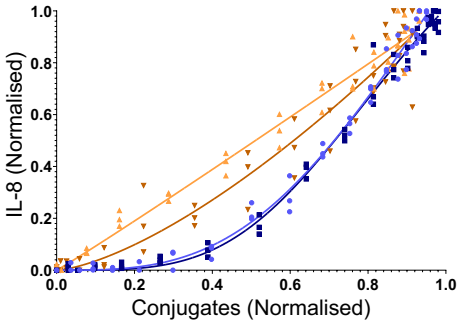

F Test	P value
SIRPß1 vs Siglec 14	0.0084
SIRPß1 vs NKp44	<0.0001
SIRPß1 vs TREM-1	<0.0001
Siglec 14 vs NKp44	<0.0001
Siglec 14 vs TREM-1	<0.0001
NKp44 vs TREM-1	0.5775

F Test	P value
SIRPß1 vs Siglec 14	<0.0001
SIRPß1 vs NKp44	0.0873
SIRPß1 vs TREM-1	<0.0001
Siglec 14 vs NKp44	<0.0001
Siglec 14 vs TREM-1	<0.0001
NKp44 vs TREM-1	0.0467

F Test	P value
SIRPß1 vs Siglec 14	0.0036
SIRPß1 vs NKp44	<0.0001
SIRPß1 vs TREM-1	<0.0001
Siglec 14 vs NKp44	<0.0001
Siglec 14 vs TREM-1	<0.0001
NKp44 vs TREM-1	0.0004

sFigure 4

A

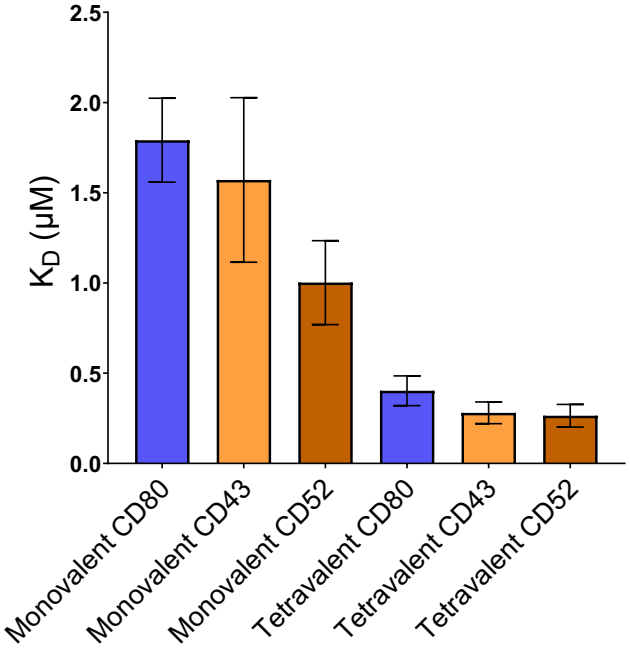
2.5
2.0
1.5
1.0
0.5
0.0
K_D (μM)
Monovalent CD80
Monovalent CD43
Monovalent CD52
Tetravalent CD80
Tetravalent CD43
Tetravalent CD52

B

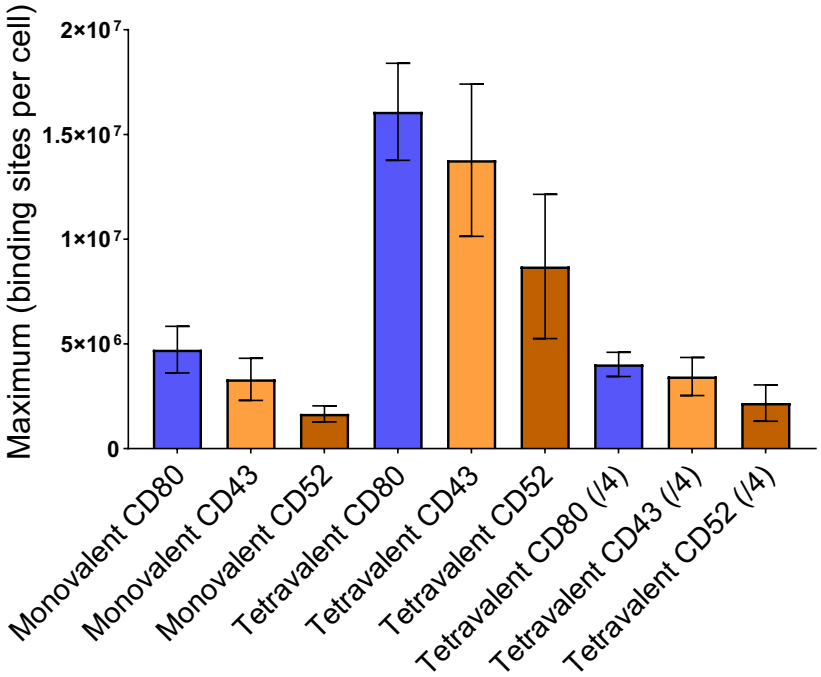
2×10^7
1.5×10^7
1×10^7
5×10^6
0
Maximum (binding sites per cell)
Monovalent CD80
Monovalent CD43
Monovalent CD52
Tetravalent CD80
Tetravalent CD43
Tetravalent CD52
Tetravalent CD80 (/4)
Tetravalent CD43 (/4)
Tetravalent CD52 (/4)

sFigure 5

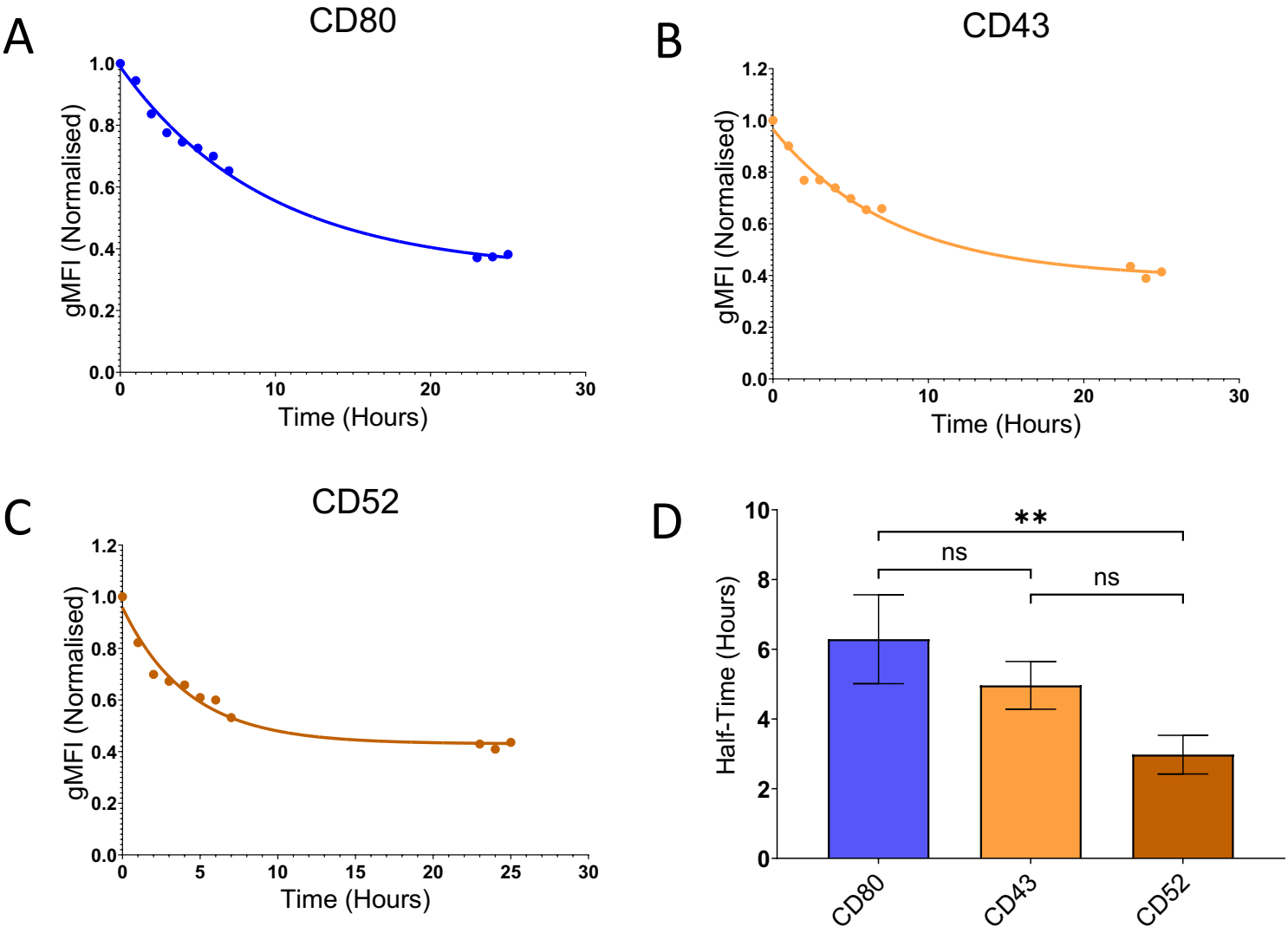
A
CD80
gMFI (Normalised)
Time (Hours)
B
CD43
gMFI (Normalised)
Time (Hours)
C
CD52
gMFI (Normalised)
Time (Hours)
D
Half-Time (Hours)
**
ns
ns
CD80
CD43
CD52

sFigure 6

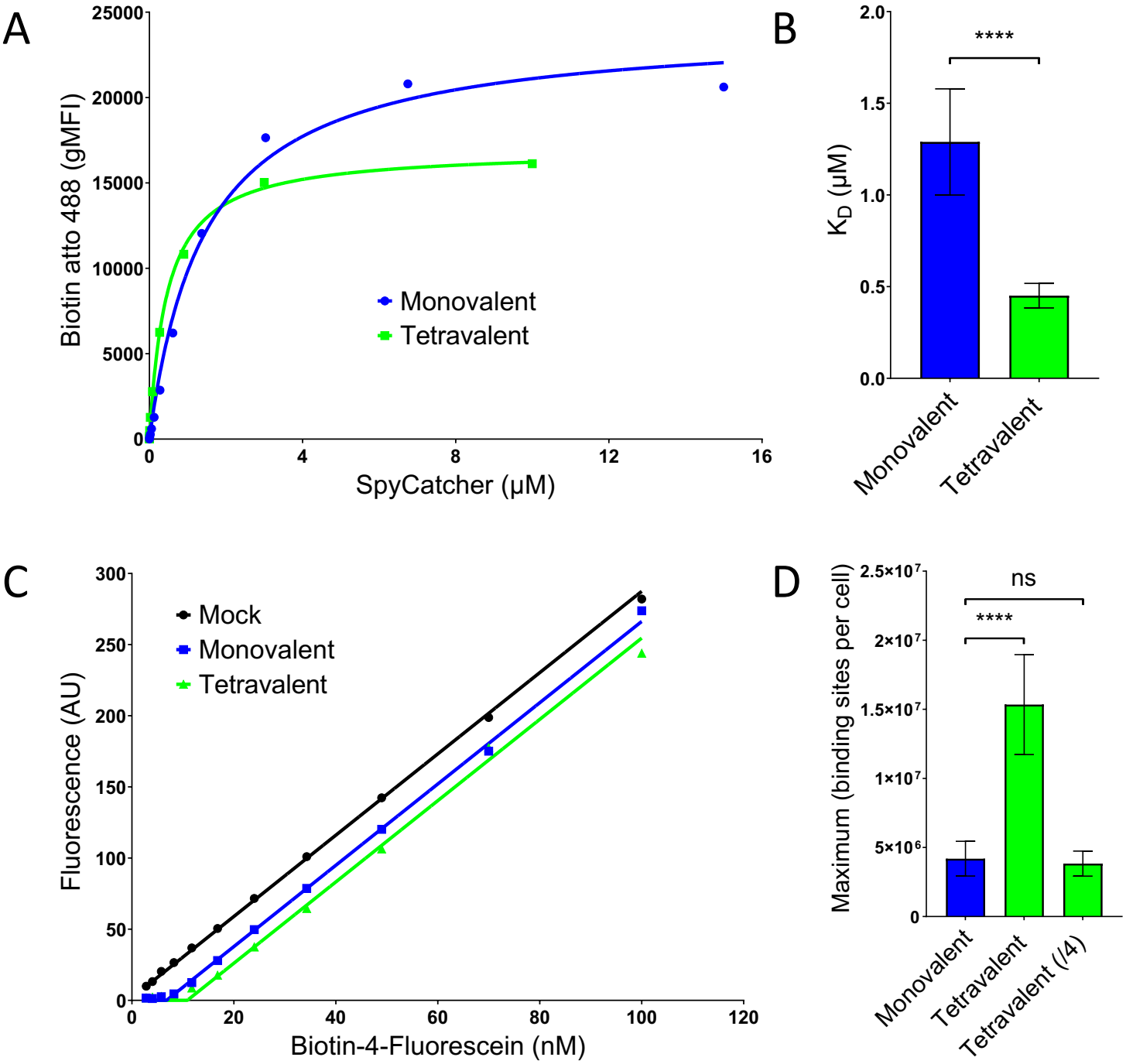
A
Biotin atto 488 (gMFI)
25000
20000
15000
10000
5000
0
0
4
8
12
16
SpyCatcher (μM)
Monovalent
Tetravalent
B
K_D (μM)
2.0
1.5
1.0
0.5
0.0
****
Monovalent
Tetravalent
C
Fluorescence (AU)
300
250
200
150
100
50
0
0
20
40
60
80
100
120
Biotin-4-Fluorescein (nM)
Mock
Monovalent
Tetravalent
D
Maximum (binding sites per cell)
2.5×10^7
2×10^7
1.5×10^7
1×10^7
5×10^6
0
ns
****
Monovalent
Tetravalent
Tetravalent (/4)

sFigure 7

A

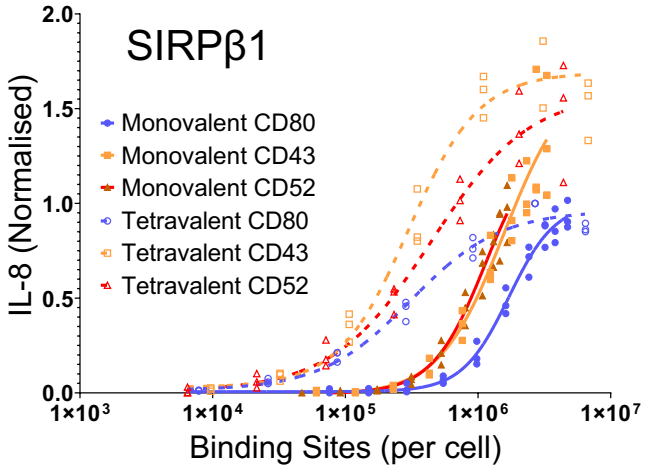

F Test	P value
CD80	<0.0001
CD43	<0.0001
CD52	<0.0001

B

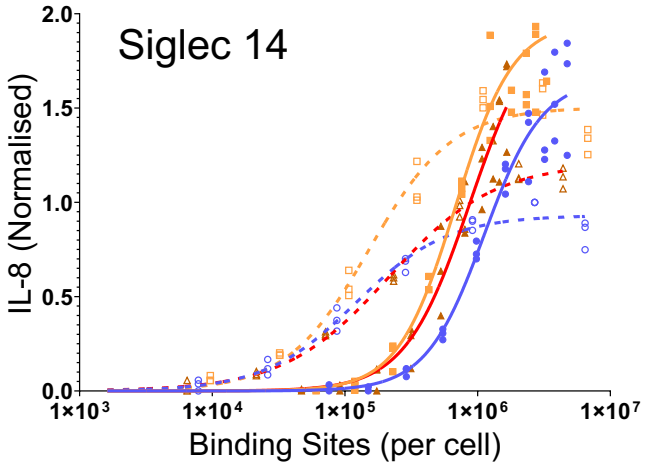

F Test	P value
CD80	<0.0001
CD43	<0.0001
CD52	<0.0001

C

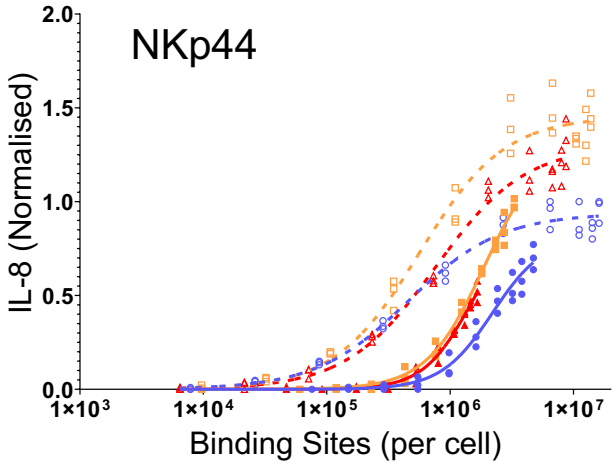

F Test	P value
CD80	<0.0001
CD43	<0.0001
CD52	<0.0001

D

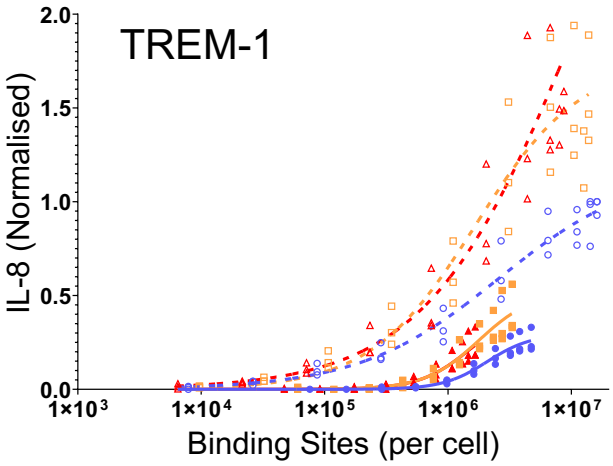

F Test	P value
CD80	<0.0001
CD43	<0.0001
CD52	<0.0001

sFigure 8

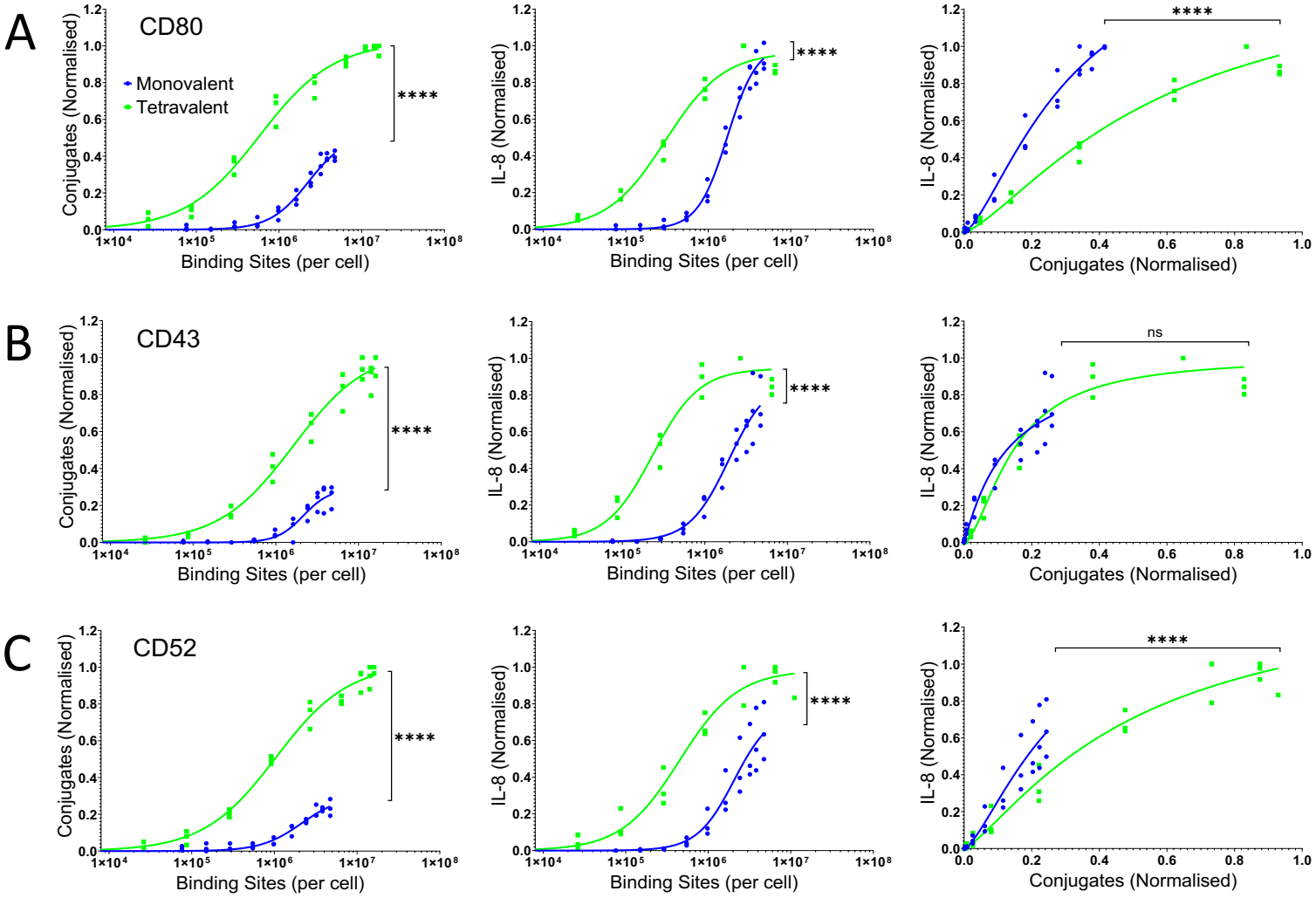
A
CD80
Monovalent
Tetravalent
Conjugates (Normalised)
Binding Sites (per cell)
****
IL-8 (Normalised)
Binding Sites (per cell)
****
IL-8 (Normalised)
Conjugates (Normalised)
****
B
CD43
Conjugates (Normalised)
Binding Sites (per cell)
****
IL-8 (Normalised)
Binding Sites (per cell)
****
IL-8 (Normalised)
Conjugates (Normalised)
ns
C
CD52
Conjugates (Normalised)
Binding Sites (per cell)
****
IL-8 (Normalised)
Binding Sites (per cell)
****
IL-8 (Normalised)
Conjugates (Normalised)
****

sFigure 9

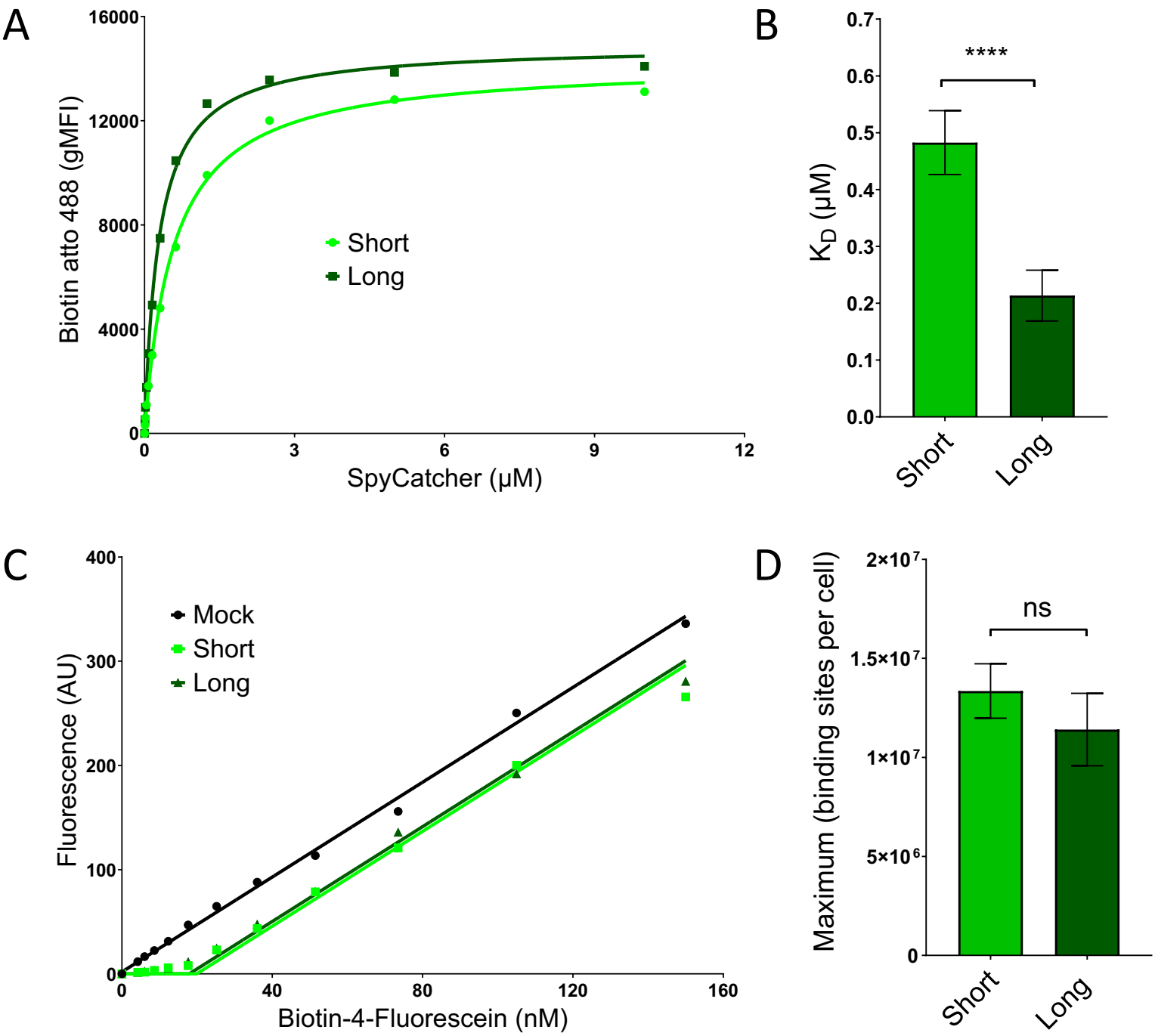
A
Biotin atto 488 (gMFI)
16000
12000
8000
4000
0
0
3
6
9
12
SpyCatcher (μM)
Short
Long
B
K_D (μM)
0.7
0.6
0.5
0.4
0.3
0.2
0.1
0.0
****
Short
Long
C
Fluorescence (AU)
400
300
200
100
0
0
40
80
120
160
Biotin-4-Fluorescein (nM)
Mock
Short
Long
D
Maximum (binding sites per cell)
2×10⁷
1.5×10⁷
1×10⁷
5×10⁶
0
ns
Short
Long